Morphine hyperalgesia gated through microglia-mediated disruption of neuronal Cl− homeostasis

Morphine hyperalgesia gated through microglia-mediated disruption of neuronal Cl^- homeostasis

Francesco Ferrini[1–3,10], Tuan Trang[4–7,10], Theresa-Alexandra M Mattioli[8], Sophie Laffray[1,2], Thomas Del'Guidice[1,2], Louis-Etienne Lorenzo[1,2], Annie Castonguay[1,2], Nicolas Doyon[1,2], Wenbo Zhang[4,5], Antoine G Godin[1,2], Daniela Mohr[4,5], Simon Beggs[4,5], Karen Vandal[1], Jean-Martin Beaulieu[1,2], Catherine M Cahill[8,9], Michael W Salter[4,5] & Yves De Koninck[1,2]

[1]Institut Universitaire en Santé Mentale de Québec, Québec, Canada. [2]Department of Psychiatry and Neuroscience, Université Laval, Québec, Québec, Canada. [3]Department of Veterinary Sciences, University of Turin, Turin, Italy. [4]Program in Neurosciences & Mental Health, Hospital for Sick Children, Toronto, Ontario, Canada, [5]Department of Physiology, University of Toronto, Toronto, Ontario, Canada. [6]Department of Comparative Biology and Experimental Medicine, University of Calgary, Calgary, Canada. [7]Department of Physiology and Pharmacology, Hotchkiss Brain Institute, University of Calgary, Calgary, Canada. [8]Department of Biomedical and Molecular Sciences, Queen's University, Kingston, Ontario, Canada. [9]Department of Anesthesiology and Perioperative Care, University of California, Irvine, California, USA. [10]These authors contributed equally to this work. Correspondence should be addressed to Y.D.K. (*yves.dekoninck@crulrg.ulaval.ca*).

A major unresolved issue in treating pain is the paradoxical hyperalgesia produced by the gold-standard analgesic morphine and other opiates. We found that hyperalgesia-inducing treatment with morphine resulted in downregulation of the K^+-Cl^- co-transporter KCC2, impairing Cl^- homeostasis in rat spinal lamina l neurons. Restoring the anion equilibrium potential [AU: Please define E_{anion}.] reversed the morphine-induced hyperalgesia without affecting tolerance. The hyperalgesia was also reversed by ablating spinal microglia. Morphine hyperalgesia, but not tolerance, required μ opioid receptor–dependent expression of P2X4 receptors (P2X4Rs) in microglia and μ-independent gating of the release of brain-derived neurotrophic factor (BDNF) by P2X4Rs. Blocking BDNF-TrkB signaling preserved Cl^- homeostasis and reversed the hyperalgesia. Gene-targeted mice in which BDNF was deleted from microglia did not develop hyperalgesia to morphine. However, neither morphine antinociception nor tolerance was affected in these mice. Our findings dissociate morphine-induced hyperalgesia from tolerance and suggest the microglia-to-neuron P2X4-BDNF-KCC2 pathway as a therapeutic target for preventing hyperalgesia without affecting morphine analgesia.

Morphine and other opiates are indispensable in the treatment of moderate-to-severe postoperative and chronic pain, but the use of these drugs is plagued by the development of two major problems: tolerance and hyperalgesia[1]. Tolerance is characterized by a progressive lack of response to morphine that can be overcome by increasing the dose, whereas hyperalgesia is a sensitization process in which opioids, paradoxically, cause pain hypersensitivity[2]. Commonly held views are that tolerance and hyperalgesia reflect a single underlying cellular and molecular mechanism[3,4].

The spinal dorsal horn (SDH) is a primary site of action for the analgesic effects of morphine and

other opiates, and has been implicated in morphine-induced hyperalgesia (MIH) and tolerance[5,6]. In the SDH, nociceptive information is received from sensory fibers, processed and relayed to brain areas involved in mediating the sensory and emotional aspects of pain[7,8]. Nociceptive processing involves neuron-neuron and neuron-glia interactions through multiple facilitatory and inhibitory signaling cascades regulating the final output of the pain signaling networks. But the manner in which morphine acts on these networks in the SDH to produce hyperalgesia or tolerance remains enigmatic.

In the SDH, lamina I neurons comprise one of the principal out- put pathways to the brain[8–10]. These neurons are central targets for opioid analgesia[5], which inhibit their activity. Conversely, increasing the output in this pathway has been implicated as a neuronal substrate underlying morphine tolerance and hyperalgesia[6,9]. Spinal nociceptive output is increased by enhanced excitation and diminished inhibition[10], and the latter has recently been implicated as a substrate of several chronic pain conditions[11]. Although morphine induces analgesia via inhibition in the SDH, we examined the seemingly counterintuitive concept that morphine may also induce disinhibition, the latter being the neuronal substrate for hyperalgesia and/or tolerance.

We found that morphine induced hyperalgesia via a P2X4R- BDNF-KCC2 disinhibition cascade between microglia and SDH neurons. Interfering with the principal nodes in the cascade sup- pressed hyperalgesia, but had no effect on tolerance. The disinhibition was a result of impaired Cl^- extrusion in lamina I neurons. Pharmacological blockade of P2X4Rs reversed hyperalgesia and mice lacking these receptors did not develop hyperalgesia. Similarly, hyperalgesia was reversed by blocking BDNF-TrkB signaling and did not develop in mice lacking BDNF in microglia. Finally, restoring hyperpolarizing inhibition reversed morphine hyperalgesia. Thus, our findings describe a signaling pathway underlying MIH, opening avenues to specifically prevent and reverse this highly deleterious effect of morphine without affecting its analgesic action.

RESULTS

To determine whether there is a common or separate mechanism for tolerance and hyperalgesia, we used a differential testing procedure in rats treated with morphine sulfate (10 mg per kg of body weight, sub- cutaneous) twice daily over 7 d. Morphine antinociception was mea- sured by testing thermal withdrawal threshold 1 h after each morning injection (n = 14 rats, $P < 0.001$; **Fig. 1a**). Although morphine induced a significant increase in thermal withdrawal threshold at that time point on day 1, the antinociception was significantly reduced within 3 d of treatment ($P < 0.001$; **Fig. 1a**). By day 5, morphine had no effect on withdrawal threshold, indicating that the rats were tolerant to the antinociceptive effects of morphine. Development of hyper- algesia was assessed separately by testing rats just before each morning injection of

morphine (**Fig. 1b**,**c**). We found a progressive decrease in withdrawal threshold over the course of 5–7 d of morphine treatment (n = 14 rats, $P < 0.001$), but not with saline injections (n = 10, $P > 0.05$; **Fig. 1b**,**c**), indicating the development of pain hypersensitivity in these animals. Pain hypersensitivity was also observed by increased responses to nociceptive stimulation: vocalizations in response to the subcutaneous injections (n = 7, $P < 0.05$; **Fig. 1d**) and licking behavior after thermal stimulation (n = 7 rats, day 7, $P < 0.05$; **Fig. 1e**) were increased by repeated morphine treatment. In contrast, no change in motor performance was observed using the accelerating rotarod test (**Fig. 1f**), indicating that the decrease in withdrawal thresholds was not a result of altered motor activity. That the time course for the development of hyperalgesia was different from that for tolerance raised the possibility that the two processes have distinct underlying mechanisms.

MIH resulted from altered Cl^- homeostasis

Disinhibition through disrupting Cl^- homeostasis is one mechanism for increasing the output of lamina I neurons in the SDH[12,13]. We investigated whether morphine alters Cl^- homeostasis in lamina I neurons. We measured the Cl^- extrusion capacity of these neurons in spinal cord slices isolated from rats receiving either saline or morphine injections for 7 d (**Fig. 2a**,**b**)[14]. Following application of an intracellular Cl^- load, we found that the reversal potential for $GABA_A$ currents, E_{GABA}, in lamina I neurons of morphine-treated rats (−42.3 ± 1.3 mV, n = 6 cells) was significantly more depolarized than that in lamina I neurons of saline-treated rats (−50.1 ± 2.2 mV, n = 5 cells, $P < 0.05$; **Fig. 2**). Because hyperalgesia may also develop within hours of high-dose treatments[15], we incubated spinal cord slices from naive rats with 1 μM morphine for 3 h. *In vitro* morphine treatment also resulted in a significant shift in E_{GABA} ($P < 0.01$; **Fig. 2c**,**d**). Thus, both repeated and high-dose morphine treatment impair Cl^- extrusion in lamina I neurons.

To separately test whether morphine weakens Cl^- extrusion, we used an established procedure involving collapse of the Cl^- gradient during trains of evoked inhibitory postsynaptic currents (eIPSCs)[16]. The contribution of Cl^- accumulation to activity-dependent depression of synaptic activity was determined by stimulating inhibitory transmission while holding the membrane potential either above (0 mV) or below (−90 mV) the Cl^- reversal potential, E_{Cl}[16]. When holding at −90 mV, the rate of decrease of eIPSC amplitude depends on activity-dependent synaptic depression, whereas the rate of decrease at 0 mV reflects synaptic depression and postsynaptic Cl^- accumulation[16]. Morphine did not affect the rate of synaptic depression at −90 mV ($P > 0.05$; **Fig. 2e**), which is consistent with the lack of presynaptic μ receptor expression in spinal inhibitory interneurons[17]. In contrast, the

decrease in eIPSC amplitude at 0 mV occurred more quickly after morphine ($P < 0.05$; **Fig. 2f**). The differential effect of morphine at 0 mV versus −90 mV indicates that morphine treatment resulted in increased Cl^- accumulation. Thus, morphine weakened Cl^- extrusion, as measured with Cl^- loaded either tonically through the patch pipette or phasically through synaptic receptors.

Further evidence of a collapse in Cl^- gradient in neurons exposed to morphine was found in the responses to exogenous GABA applied in the presence of physiological $[Cl^-]_i$ in cells held near the resting potential (−60 mV; **Fig. 2g**). In these neurons, GABA evoked a biphasic response, an initial outward current followed by a shift to an inward current (**Fig. 2g**), as previously described in neurons with impaired Cl^- extrusion capacity[14,18]. In contrast, in lamina I neurons that were not exposed to morphine, the response to GABA remained outward at −60 mV (**Fig. 2g**). The inward component of the response to GABA has been associated with outward flux of HCO_3^- becoming predominant when the Cl^- gradient collapses, yielding a progressive depolarizing shift in E_{GABA}[14,19,20]. To determine whether this was the case in neurons exposed to morphine, we bath-applied acetazolamide (ACTZ, 50 μM), a cell-permeant inhibitor of carbonic anhydrase, the enzyme responsible for generating HCO_3^- intracellularly[20]. In the presence of ACTZ, the GABA response remained outward, yielding a 10 mV hyperpolarizing shift in E_{GABA}, measured 1 s after the onset of the GABA puff (**Fig. 2g**). These findings are consistent with ACTZ lowering the generation of HCO_3^-, resulting in an activity-dependent depletion of HCO_3^- and ensuing loss of HCO_3^- efflux, during the GABA response[20] (**Supplementary Fig. 1**).

Preventing the progressive shift in E_{GABA} in neurons with impaired Cl^- extrusion substantially restores inhibition[19,21]. Thus, ACTZ may mitigate the effect of the morphine-induced collapse in Cl^- gradient, rescuing the impairment of inhibition. We tested the effects of intrathecal administration of ACTZ in rats with established hyper- algesia after 7–9 d of morphine treatment. ACTZ administration reversed morphine-induced mechanical and thermal hypersensitivity (**Fig. 2h**). We conclude that ACTZ reversed the hyperalgesia by reducing HCO_3^--mediated inward current, thereby restoring E_{GABA}. Taken together, our findings indicate that altered anion homeostasis underlies MIH.

Morphine reduces Cl^- transport and KCC2 expression

In adult lamina I neurons, Cl^- homeostasis is mainly regulated by the K^+-Cl^- co-transporter, KCC2 [12,22]. We examined the effect of repeated morphine treatment on spinal KCC2 expression. After 7 d of morphine treatment, there was a significant decrease in KCC2 immunoreactivity in lamina I of morphine-treated rats (103.4 ± 5.8 intensity units (i.u.), $n = 5$ rats) compared with that of saline-treated rats (191.2 ± 5.8 i.u., $n = 5$ rats, $P < 0.01$; **Fig. 3a**). In addition, KCC2 protein levels in SDH

homogenates were reduced by morphine (**Fig. 3b**). As KCC2 oligomerization may be critical for transporter function[23], we analyzed the KCC2 oligomer to monomer ratio in the absence of detergents and found that the ratio was significantly reduced in the SDH of morphine-treated rats ($P < 0.05$; **Fig. 3c**). In contrast, morphine had no effect on KCC2 expression or oligomer to monomer ratio in the spinal ventral horn (**Fig. 3b**,**c**). Thus, the morphine- induced impairment in Cl^- homeostasis in lamina I neurons may result from a loss of the oligomeric form of KCC2 in these cells.

To test whether total KCC2 activity in lamina I neurons is affected by morphine, we examined the transporter activity in reverse mode[24] by measuring K^+-driven uptake of Cl^-. We performed intracellular Cl^- imaging and stepped extracellular K^+ from 2.5 to 15 mM in control or morphine-treated slices (1 μM for 3 h; **Fig. 3d**,**e**). The rate of Cl^- accumulation was significantly lower in morphine-treated neurons ($n = 8$ cells, 0.32 ± 0.04 $\%\Delta F/F$ per s) than in control neurons ($n = 8$ cells, 0.54 ± 0 0.2 $\%\Delta F/F$ per s, $P < 0.05$; **Fig. 3e**). These data indicate that morphine impairs Cl^- homeostasis by reducing KCC2-mediated Cl^- transport.

MIH, but not tolerance, requires spinal microglia

Because microglia have been implicated in disrupting Cl^- homeo- stasis in lamina I neurons[22,25], we asked whether MIH may differentially depend on spinal microglia. We found that repeated morphine treatment induced an increase in CD11b immuno- reactivity, which is specifically expressed by microglia in the CNS (**Fig. 4a**), indicating that spinal microglia respond to morphine treatment. To determine whether spinal microglia are required for morphine tolerance or hyperalgesia, we depleted microglia in the spinal cord of morphine-treated rats using intrathecal injection of a saporin-conjugated antibody to Mac1[26] (**Fig. 4b**). Intrathecal injections were begun on day 7, when both pain hypersensitivity and morphine tolerance had been established. Within 2 d, saporin- conjugated antibody to Mac1 (20–36 μg), but not saporin alone (20 μg), reversed morphine-induced thermal pain hypersensitivity ($n = 6$ saporin-treated rats, $n = 7$ antibody to Mac1– and saporin- treated rats, $P < 0.01$; **Fig. 4c**). Saporin-conjugated antibody to Mac1 also reversed morphine-induced mechanical allodynia (mechanical threshold at day 7 of morphine injection, 0.4 ± 0.1 of the baseline, $n = 5$; mechanical threshold at day 8 of morphine injection following intrathecal antibody to Mac-1 and saporin administration, 1.2 ± 0.3 of the baseline, $n = 5$ rats; $P < 0.05$). In contrast, saporin- conjugated antibody to Mac-1 had no effect on morphine tolerance ($P > 0.05$; **Fig. 4d**). Thus, we conclude that microglia in the SDH are necessary for the ongoing expression of hyperalgesia, but not for tolerance caused by repeated morphine treatment.

To determine whether morphine-treated microglia are sufficient to produce pain hypersensitivity, we used an *in vivo* microglia transfer approach[22,27]. Microglia in primary culture were chronically treated

with morphine and then injected intrathecally at the lumbar spinal level in naive rats (**Fig. 5a**). We found that mechanical withdrawal threshold was markedly decreased after intrathecal administration of morphine-treated microglia (n = 7 rats, $P < 0.001$; **Fig. 5a**). In contrast, mechanical withdrawal threshold was unaffected by saline-treated microglia. Thus, morphine-treated microglia are sufficient to cause pain hypersensitivity in naive animals.

Microglial P2X4 receptors are required for MIH

Pain hypersensitivity produced by microglia critically depends on P2X4 receptors (P2X4Rs)[27], suggesting that morphine-induced pain hypersensitivity may require microglial P2X4Rs. We found that the decrease in withdrawal threshold produced by transfer- ring morphine-treated microglia was prevented by TNP-ATP, an antagonist of P2X1R, P2X2R, P2X3R and P2X4R, but not by PPADS, an antagonist of P2X1R, P2X2R, P2X3R, P2X5R and P2X7R[27], implicating P2X4Rs in the expression of the pain hypersensitivity evoked by morphine-treated microglia (**Fig. 5a**). Moreover, we found that repeated morphine treatment did not induce a change in thermal and mechanical withdrawal threshold, licking time or vocalization in *P2rx4*$^{-/-}$ mice (**Fig. 5b**–**d**); however, *P2rx4*$^{+/+}$ mice developed multiple signs of pain hypersensitivity in response to morphine (**Fig. 5b**–**d**). Thus, P2X4Rs are required for the development of hyperalgesia. To test whether P2X4Rs are also necessary for the ongoing expression of hyperalgesia, we administered TNP-ATP (30 nmol) intrathecally in morphine-treated mice. We found that TNP-ATP reversed the decrease in thermal withdrawal threshold that had developed after 7 d of morphine treatment (**Fig. 5e**) without affecting morphine tolerance (**Fig. 5f**). In another series of experiments, intrathecal TNP-ATP administration also reversed established mechanical allodynia in morphine-treated rats (**Fig. 5g**).

As our findings suggest that P2X4Rs are required for the development and ongoing expression of hyperalgesia resulting from morphine treatment, we questioned whether morphine treatment may increase P2X4R expression, which is normally present at low levels in the naive CNS[27,28]. In *P2rx4*$^{-/-}$ mice, in which *P2rx4* was replaced with *lacZ*, we found a greater X-gal (5-bromo-4-chloro-indolyl-galactopyranoside) signal in the spinal cord of morphine-treated than in saline-treated mice (**Fig. 5h**). Moreover, we found that repeated morphine treatment increased P2X4R protein expression in wild-type mice (see below). To determine whether morphine may act directly on microglia, we used primary microglia cultures and found that chronic morphine treatment resulted in an increase in P2X4R protein expression (**Fig. 5i**). These receptors were functional, as indicated by morphine-induced increases in P2X4R-mediated currents (**Fig. 5j**) and Ca^{2+} responses (see below). Thus, MIH depends on P2X4Rs, and morphine treatment induces an increase in *P2rx4* gene expression autonomously in microglia.

MIH, but not tolerance, requires microglial BDNF

Stimulation of P2X4Rs in microglia evokes the release of BDNF[22,29,30], which is known to downregulate KCC2 expression in adult neurons[31]. Thus, we asked whether morphine treatment causes a P2X4R-dependent release of BDNF from microglia. We found that chronic morphine treatment resulted in the release of BDNF from primary microglia cultures (**Fig. 6a**). The morphine-evoked release of BDNF was blocked by TNP-ATP, but was unaffected by PPADS (**Fig. 6a**). BDNF release was also blocked by the ATP-degrading enzyme apyrase (**Fig. 6a**), indicating that morphine causes the release of BDNF through ATP-mediated stimulation of P2X4Rs. The mechanical hypersensitivity evoked by morphine-treated microglia was prevented by a BDNF-sequestering fusion protein (TrkB-Fc)[32], but not by the control peptide IgG-Fc (**Fig. 6b**). Together, our findings indicate that morphine treatment results in P2X4R-dependent release of BDNF from microglia, which is sufficient to induce pain hypersensitivity.

We then addressed whether BDNF and signaling through its cognate receptor TrkB are necessary for morphine-induced impairment of the Cl^- extrusion capacity of lamina I neurons and ensuing hyperalgesia. The shift in E_{GABA} induced by morphine treatment was prevented by co-incubation with a function-blocking antibody to TrkB (**Fig. 6c**,**d**). To determine whether BDNF-TrkB signaling is required for the ongoing expression of MIH, we tested the effects of intrathecal injections of a function-blocking anti- body to TrkB. The antibody produced a gradual reversal of thermal hyperalgesia over 3 d in rats that had been treated with morphine for 7 d, comparable to that obtained by ACTZ treatment (**Fig. 6e**); however, neither antibody to TrkB nor ACTZ affected morphine antinociception (**Fig. 6f**), indicating that BDNF and the associated disrupted Cl^- homeostasis are required for ongoing expression of MIH, but not of tolerance.

To determine whether the requisite BDNF is released from microglia, we used gene-targeted mice in which BDNF was deleted in microglia. These mice were generated by crossing mice expressing Cre recombinase under the control of the *CD11b* (also known as *Itgam*) promoter (*CD11b-cre*) with those in which exon 5 of the *Bdnf* gene, which encodes the BDNF protein, was flanked by *loxP* sites ($Bdnf^{loxP/loxP}$) yielding *CD11b-cre;* $Bdnf^{loxP/loxP}$ mice[33,34]. Lumbar spinal activity of the *CD11b-cre* transgene was verified by crossing mice with *Rosa26* mice, which ubiquitously express the β-galactosidase (β-gal) transgene[33]. Microglia, but not neurons or astrocytes, expressed β-gal in *Rosa26; CD11b-cre* mice. In addition, Cre expression was detected only in cells that expressed the microglial markers Iba-1 and CD11b (S.B., T.T., J. Alexander and M.W.S., unpublished observation). No differences in mechanical nociceptive behavior were observed between *CD11b-cre;* $Bdnf^{loxP/loxP}$ mice (1.5 ± 0.2 g, n = 7 mice) and their littermate $Bdnf^{loxP/loxP}$ controls (1.5 ± 0.2 g, n = 7 mice; $P > 0.05$). However, only $Bdnf^{loxP/loxP}$ mice developed robust

hyperalgesia following repeated morphine treatment, and we found no change in mechanical withdrawal threshold, licking time or vocalization in *CD11b-cre; Bdnf*$^{loxP/loxP}$ mice (**Fig. 7a**–**c**). *CD11b-cre; Bdnf*$^{loxP/loxP}$ mice were indistinguishable from *Bdnf*$^{loxP/loxP}$ mice with regard to a peak antinociceptive response to a single dose of mor- phine (**Fig. 7d**), progressive increase in median effective dose (ED50) to escalating morphine doses, shift in the morphine dose-response curve following 5 d of morphine treatment (**Fig. 7e**) or expression of naloxone-precipitated signs of withdrawal (**Fig. 7f**). Thus, acute morphine antinociception, tolerance and withdrawal behavior were not altered in the *CD11b-cre; Bdnf*$^{loxP/loxP}$ mice. We conclude that BDNF from microglia is required specifically for the hyperalgesia induced by morphine.

Both μ-dependent and μ-independent signaling are necessary

The simplest cascade of events that could account for our findings is that the hyperalgesia induced by morphine is driven by increased expression of P2X4Rs in microglia leading to a release of BDNF that acts through TrkB receptors to downregulate functional expression of KCC2 with subsequent disruption of Cl^- homeostasis in lamina I neurons. This raises the question of what are the direct molecular targets of morphine and their location, or locations, in this core pathway. The direct molecular target for morphine-induced analgesia are the well-known seven transmembrane isoforms of the μ opioid receptor[35]. Expression of μ receptors is evident in spinal microglia[36] (**Supplementary Fig. 2**). On the other hand, there is increasing evidence that the actions of morphine or its metabolites may be dependent on concurrent activation of μ receptor– independent pathways[37,38]. To test this possibility, we examined the effects of stereoisomers of the opioid receptor antagonist naloxone. (−)Naloxone blocked both μ-mediated and non–μ-mediated signaling, and (+)naloxone blocked only the non–μ-mediated mechanisms[37]. We found that spinally administered (+)naloxone prevented morphine hyperalgesia (**Fig. 8a**), but did not affect the development of tolerance (**Fig. 8b**). Moreover, (+)naloxone reduced morphine-induced upregulation of CD11b (**Fig. 8c**) and prevented the shift in E_{GABA} in lamina I neurons in spinal slices treated with morphine (n = 8 cells, $P > 0.05$; **Fig. 8d**). Finally, (+)naloxone prevented the hyperalgesic action of intrathecal administration of morphine-treated microglia (**Fig. 8e**). Thus, μ receptor–independent signaling is essential for the microglia-neuron interactions that cause hyperalgesia.

To examine whether morphine targets microglia specifically, we tested naloxone stereoisomers in cultured microglia that are competent to transfer hyperalgesia. Morphine-induced increases in P2X4R expression and function in microglia cultures were blocked by (−)naloxone, but were unaffected by

(+)naloxone (**Fig. 8f**,**g**). Similarly, the increase in spinal P2X4R expression caused by repeated morphine administration *in vivo* was prevented by (−)naloxone, but not by (+)naloxone (**Fig. 8h**). The morphine-induced increase in microglial P2X4Rs therefore required μ opioid receptors. However, morphine-evoked release of BDNF in microglia cultures in which P2X4R expression was already upregulated was prevented by (+)naloxone (**Fig. 8i**). Thus, we conclude that, in microglia, μ receptors mediate the upregulation of P2X4Rs and a μ receptor–independent mechanism is required for the morphine-stimulated release of BDNF.

The mechanisms of μ receptor–independent signaling by morphine are not fully understood. It has been suggested that Toll-like receptor 4 (TLR4) mediates morphine-induced neuroinflammatory responses[39]. To test the potential involvement of TLR4, we measured morphine- induced release of BDNF from microglia cultures in the presence of the TLR4 antagonist LPS-RS (lipopolysaccharide from *Rhodobacter sphaeroides*)[39]. Across a range of concentrations, LPS-RS had no effect on morphine-induced release of BDNF (**Fig. 8j**), consistent with our previous finding that LPS treatment does not induce BDNF release from microglia[29]. In addition, we found that mice lacking functional TLR4 (C3H/HeJ mice) developed tactile hypersensitivity with mor- phine treatment that was indistinguishable from that of wild-type controls (C3H/HeOuJ mice; **Fig. 8k**). These findings indicate that TLR4 is not required for morphine hyperalgesia.

DISCUSSION

Our findings suggest a pathway by which morphine produces hyperalgesia, which ultimately occurs via the dysregulation of Cl^- homeostasis in pain-signaling neurons in spinal lamina I. The most parsimonious interpretation is that this pathway is initiated by mor- phine acting on μ-opioid receptors in SDH microglia, which, through release of BDNF, signal the lamina I neurons, inducing Cl^- dysregulation by reducing the expression of KCC2. Although, as with hyperalgesia, morphine tolerance is dependent on μ receptors[40], our results indicate that microglia and the subsequent components of the hyperalgesia pathway are not required for tolerance. That hyperalgesia and tolerance are mechanistically distinct is consistent not only with the observation that tolerance and hyperalgesia have differing clinical characteristics[41], but also with recent findings uncovering the signaling pathways underlying morphine tolerance, which do not affect hyperalgesia[42]. Our results also suggest that the mechanism that we uncovered represents a substrate of ongoing hyperalgesia induced by morphine rather than withdrawal hyperalgesia.

A key concept emerging from our findings is that morphine causes disinhibition by disrupting neuronal Cl^- homeostasis. However, morphine is currently perceived as causing inhibition either pre- or postsynaptically. Thus, morphine-induced spinal disinhibition is a previously unknown mechanism for the actions of this drug and other opiates. We found that, in the SDH, this disinhibition led to the paradoxical hyperalgesic action of morphine. A therapeutic avenue that follows from this finding to prevent or reverse selectively the hyperalgesia is to restore $GABA_A$ and/or glycine receptor–mediated inhibition, which could be achieved by enhancing $GABA_A$ receptor activation through positive modulation, such as with benzodiazepines[43]. This strategy may be of limited efficacy, however, given our finding that disinhibition results from dysregulation of Cl^- homeostasis. Indeed, if E_{GABA} is depolarized beyond a certain point, enhancing $GABA_A$ transmission may become counterproductive[21]. In such conditions, restoring E_{GABA} by blocking the carbonic anhydrase to attenuate the depolarizing HCO_3^- component of $GABA_A$- and glycine-mediated currents could potentially reverse morphine hyper- algesia, as has been done to improve the anti-hyperalgesic potency of benzodiazepines[44]. Activity-dependent accumulation of Cl^- through $GABA_A$ or glycine channels resulting from compromised Cl^- extrusion capacity will nevertheless provoke some breakdown of inhibition with the above approaches[19]. Thus, restoring Cl^- extrusion capacity through enhancing KCC2 expression or activity[31] will likely be more effective as an adjuvant therapy to chronic morphine treatment.

Disinhibition and hyperalgesia caused by morphine treatment are mediated by upregulation of P2X4Rs in the spinal cord microglia *in vivo*, driving synthesis and release of BDNF[29,30]. Morphine has been found to upregulate P2X4Rs[45] and to induce BDNF transcription[46] via μ receptors in microglia *in vitro*. These findings point to a role for μ receptor activation in the microglia signaling cascade leading to hyperalgesia. However, we found that, although μ receptor activation induced P2X4R upregulation, μ receptor–independent signaling was necessary for the subsequent BDNF release. In contrast with previous findings[39], our results do not support an involvement of TLR4 in this mechanism. This apparent discrepancy may be a result of the much lower doses of morphine that we used, although more work is needed to define the underlying pharmacology. P2X4R-dependent and μ receptor–independent pathways represent strategic targets for the pharmacological prevention of MIH, as their activation can be blocked without interfering with μ receptor–mediated analgesia[37].

Our results also reveal that the spinal disinhibition underlying MIH results from BDNF-TrkB signaling[47]. Inflammatory and neuropathic pain also depend on BDNF-TrkB signaling. Yet, in inflammatory pain, BDNF arises from primary afferents[48], whereas neuropathic pain hypersensitivity depends on BDNF

being produced by microglia[22,30]. In both MIH and neuropathic pain, the synthesis and release of BDNF from microglia requires P2X4R upregulation[29,30], in contrast with inflammatory pain. Thus, our results indicate that MIH shares a common etiology with neuropathic pain.

Our results establish an unexpected commonality in mechanisms between MIH, pain hypersensitivity after peripheral nerve injury[22] and the sequelae of spinal cord injury[49]. Altered Cl^- homeostasis, which causes depolarizing $GABA_A$-mediated events, may also contribute to NMDA receptor plasticity[12,25], thereby favoring the onset of opioid-induced long-term potentiation in spinal neurons[9]. Moreover, our findings may extend to mechanisms involved in morphine-induced drug dependence in critical reward centers of the brain. For example, BDNF causes a switch from $GABA_A$-mediated inhibition to excitation, suggestive of altered Cl^- homeostasis, in the ventral tegmental area in opiate-dependent rats[50]. Neuronal dysfunction in the mesolimbic reward pathways is considered to be an important mechanism underlying addiction. Thus, our discovery may provide a new perspective on drug dependence, in that it may involve cross talk between microglia and neurons leading to neuronal disinhibition in key brain regions that underlie reward and addiction.

Morphine hyperalgesia can no longer be seen as an inevitable consequence of morphine analgesia or tolerance. Of particular importance to therapeutic development, we found that continuous activation of this signaling pathway is necessary to specifically maintain MIH, whereas there was no effect on tolerance or withdrawal. We found that it is possible to reverse what causes the established pain hypersensitivity, potentially alleviating opiate use liability. Notably, this can be accomplished by targeting nonclassical opioid receptors or by restoring Cl^- homeostasis in SDH neurons, sparing morphine analgesia mechanisms. Taken together, our findings and the recent demonstration of a distinct mechanism underlying morphine tolerance[42] overturn the traditional dogma of the common mechanism underlying both morphine tolerance and hyperalgesia and establish a basis for a new approach to enhancing the utility of morphine in treating chronic pain.

METHODS

Animals. Adult male mice and rats (>postnatal day 60, P60) were used. Rats and mice were housed under a 12-h:12-h light/dark cycle. All experimental procedures were performed in accordance with guidelines from the Canadian Council on Animal Care.

chronic morphine protocol and behavioral models. Morphine sulfate (morphine, Sandoz) was injected twice a day (9 a.m. and 6 p.m.) into Sprague- Dawley rats (10 mg per kg), *P2rx4*$^{+/+}$ or *P2rx4*$^{-/-}$ C57BL/6 mice (F. Rassendren[51], INSERM; escalating doses from 10 to 40 mg per kg), *CD11b-cre; Bdnf*$^{loxP/loxP}$ or

Bdnf$^{loxP/loxP}$ mice (escalating doses from 10 to 40 mg per kg), C3H/HeOuJ mice (TLR4 wild type), or C3H/HeJ (functionally deficient TLR4 mutant) mice (escalating doses from 10 to 40 mg per kg, Jackson Laboratory[52]). Morphine was injected subcutaneously, unless otherwise stated. Thermal pain threshold was measured by the Hargreaves plantar test before and 1 h after morphine injection. Morphine antinociceptive effects measured 1 h after injection in chronically treated rats are not explained by altered metabolism[53]. Mechanical pain threshold was measured before morphine injection by von Frey hairs, as described previously[12]. Values are normalized to the control. Vocalizations were monitored during subcutaneous injections and differences in the relative number of vocalizing rats (%) or in the number of vocalizations (in mice) were analyzed. Licking time was measured during thermal or mechanical stimulation of the hindpaw. Motor coordination was measured by accelerating rotarod (IITC Life Science) before and 30 or 60 min after morphine injections. In a subset of experiments, a morphine cumulative dose-response curve was measured on day 6 to determine morphine ED50 value. Briefly, mice were given ascending doses of morphine every 30 min and the response to morphine was assessed by the thermal tail- flick test until a maximal level of antinociception was reached. In all behavioral studies, experimenters were blind to the drug treatments and genetic profile of rats and mice.

Behavioral assessment of naloxone-precipitated withdrawal. Mice received intraperitoneally ascending doses of systemic morphine at 8 h intervals (day 1, 10 and 20 mg per kg; day 2, 25 and 30 mg per kg; day 3, 35 and 40 mg per kg; day 4, 45 and 50 mg per kg). On day 5, mice received a morning injection of 55 mg per kg and 2 h later naloxone (2 mg per kg) to precipitate withdrawal. Control mice received saline and were challenged with naloxone on day 5. Mice were accli-matized to a clear Plexiglass testing chamber 1 h before naloxone. Signs of withdrawal were compiled as previously described[54]. Briefly, jumping, headshakes, wet-dog shakes and grooming behavior were evaluated at 10-min intervals for a total testing period of 30 min and a standardized score of 0 to 3 was assigned (0 = absent; 1 = 1–3 bouts; 2 = 4–6 bouts; 3 = 7 bouts and greater). Paw tremors, piloerection, salivation and ejaculation were also evaluated, with one point being given to the presence of each sign during each 10-min interval. The number of periods showing the latter signs were then counted (maximum score of 3 per behavioral sign) and the scores were added together to yield a final cumulative withdrawal score. Mice were also weighed before and after naloxone challenge and weight loss (an indicator of micturition and defecation) was calculated.

Generation of cd11b-cre; Bdnf$^{loxP/loxP}$ mice. Mice with microglial lineage– specific excision of BDNF were generated using the Cre-*loxP* system. C57BL/6J mice, heterozygous for *CD11b-cre* were purchased from the European Mutant Mouse Archive (provided by G. Kollias, Alexander Fleming Biomedical Research Center)[33]. 129S4/SvJae mice homozygous for *loxP*-flanked BDNF (Bdnf^{tm3Jae}/J) were purchased from

Jackson (stock 00439). These mice have *loxP* sites flanking exon 5 of the *Bdnf* gene[34]. Homozygous $Bdnf^{tm3Jae/J}$ mice were crossed with heterozygous *CD11b-cre* mice and Cre-expressing progeny backcrossed with homozygous $Bdnf^{tm3Jae/J}$ mice to ensure all experimental mice were homozygous for $Bdnf^{tm3Jae/J}$ and matched for background strains. Mice were genotyped by PCR analysis. *CD11b-cre;* $Bdnf^{loxP/loxP}$ mice exhibit normal nociceptive responses under control conditions.

Intrathecal injections. In a subset of experiments (where indicated), rats were subject to drug administration via intrathecal catheters. Rats were anesthetized with 4% isoflurane (vol/vol) and a catheter was inserted into the intrathecal space as described[55]. Unless otherwise stated, intrathecal injections were delivered 30 min before subcutaneous morphine or saline injections. Rats were tested 20 min after intrathecal injection (immediately before morphine or saline injection) and 1 h later. At the end of the experiment, the correct placement of the catheter was verified. Drugs included saporin (20 µg) and saporin-conjugated antibody to Mac-1 (16–32 µg, Advanced Targeting Systems), antibody to TrkB (30 µg, R&D Systems), ACTZ (22.5 µg, Sigma), TNP-ATP (2′,3′-O- (2,4,6-trinitrophenyl)adenosine 5′-triphosphate, 30 nmol, Tocris), naloxone (5 ng, Sigma) and (+)-naloxone (5 ng, C.J. Evans, National Institute on Drug Abuse). All drugs were dissolved in a HEPES-buffered ringer (pH 7.8).

Rat spinal cord slice preparation. Parasagittal slices (300 µm) of the rat spinal cord were prepared, as described[12]. Slices were allowed to recover for 1 h in artificial cerebrospinal fluid (ACSF) containing 126 mM NaCl, 2.5 mM KCl, 2 mM $MgCl_2$, 2 mM $CaCl_2$, 1.25 mM NaH_2PO_4, 26 mM $NaHCO_3$ and 10 mM glucose.

Patch-clamp recordings from rat lamina I neurons. Voltage-clamp recordings were performed as described previously[12]. For whole-cell experiments involv- ing measurements of E_{GABA} under Cl^- load, the intrapipette solution contained 115 mM potassium methylsulfate, 25 mM KCl, 2 mM $MgCl_2$, 10 mM HEPES, 4 mM Na-ATP, 0.4 mM Na-GTP and 0.1% Lucifer Yellow (wt/vol), pH 7.2. For whole-cell experiments to study eIPSCs, the intrapipette solution also contained 135 mM potassium methylsulfate, 5 mM KCl, 0.5 mM EGTA. For perforated patch-clamp recordings, the intrapipette solution contained 115 mM potassium methylsulfate, 25 mM KCl, 2 mM $MgCl_2$, 10 mM HEPES, 0.1% Lucifer Yellow and 30 µg ml^{-1} gramicidin (Sigma), pH 7.2. Membrane potential measurements were corrected for liquid junction potential. Data were filtered at 5 kHz, digi- tized and acquired using the Strathclyde electrophysiology software (J. Dempster, University of Strathclyde). GABA (1 mM) was puffed locally for 30 ms. The puff pipette was aimed toward the center of the neuronal somata, approximately 5 µm from the recording pipette. Experimental E_{GABA} was extrapolated from the $GABA_A$ *I-V* relationships. The difference between the experimental and the theoretical E_{GABA} (according to the Hodgkin-Katz-Goldman equation) provides an

estimate of Cl^- extrusion capacity as described[14]. Recordings of repeated eIPSCs were performed in the presence of bath-applied 6-cyano-7-nitroquinoxaline- 2,3-dione (CNQX, 10 µM) and d(−)-2-amino-5-phosphonovaleric acid (AP5, 40 µM). IPSCs were evoked by focal electrical stimulation (100 µA, 200 µs). Trains of stimuli (25 pulses, 20 Hz) were delivered every 20 s at 0 or −90 mV. Ten consecutive trains were averaged for subsequent analysis. In electrophysiological experiments, only neurons with resting membrane potential less than −50 mV and stable access resistance were included for subsequent analysis. No differences in access resistance were observed between morphine-treated (19.3 ± 0.9 MΩ) and untreated neurons (20.2 ± 1.1 MΩ). At the end of each recording session, a photograph of the recorded neuron was acquired. Data analysis was performed off-line with Clampfit 10.2 (Molecular Devices).

Imaging of reverse Cl^- transport in rat lamina I neurons. Rat spinal cord slices were labeled in ACSF containing 5 mM of the Cl^- indicator MQAE (N- 6-methoxyquinolinium acetoethylester, Molecular Probes) and 0.2% pluronic (wt/vol) in DMSO (Sigma) for 40–45 min at 20–25 °C. Slices were then trans- ferred to a perfusion chamber (2 ml min^{-1}) and extracellular MQAE was washed out for 30 min in the presence of 1 µM tetrodotoxin, 10 µM CNQX, 40 µM AP5, 1 µM strychnine and 20 µM bicuculline to minimize KCC2-independent Cl^- transport. MQAE fluorescence was measured using a Zeiss LSM 510 laser-scanning microscope coupled to a femtosecond-pulsed Ti-Sapphire laser (Chameleon Ultra, Coherent) tuned at 750 nm. Fluorescence was acquired through a 40× water-immersion objective (Zeiss, 0.8 NA) and a band-pass filter (390–465 nm). Recorded cells were identified as lamina I cells merging transmit- ted light and MQAE fluorescence. MQAE images were acquired every 5 s. After a control period of 75 s, perfusion solution was switched to ACSF containing 15 mM KCl (osmolarity adjusted using mannitol) to reverse Cl^- transport[24]. The average fluorescence from each cell body was expressed as $\%\Delta F/F_0$. Fluorescence lifetimes were measured in control and after Cl^- equilibrium was achieved in 15 mM extracellular KCl to obtain quantitative estimates of $[Cl^-]_i$ subject to drug administration via intrathecal catheters. Rats were anaesthetized independent of $[MQAE]_i$[19]. To ensure that measurements of rates of intracellular Cl^- loading were performed for comparable $[Cl^-]_i$, we initiated exposure to 15 mM KCl after sufficient incubation time so that the steady-state $[Cl^-]_i$ was comparable in control and morphine conditions. MQAE lifetime was recorded with a Becker & Hickl SPC-830 module through the nondescanned port of the Zeiss LSM 510 using a band-pass filter (469/35 nm, Semrock) coupled to a laser block (short-pass 750 nm, Semrock). Photon emission was detected using a PMC-100-1 photosensor (Hamamatsu). Lifetime in each cell was averaged over the cell body area and extracted using SPCImage software (Becker & Hickl). Instrument response function of the detection path was acquired using an 80-nm gold nanoparticle suspension to generate second-

harmonic signal. Absolute $[Cl^-]_i$ was calculated from a calibration of the Cl^- dependence of MQAE lifetime as described[19].

microglia primary culture preparation. Primary culture was prepared as described[27]. Briefly, mixed glial culture was isolated using P1–3 rat cortex and maintained for 10–14 d in DMEM medium containing 10% fetal bovine serum (vol/vol, Invitrogen). Microglia separated by gentle shaking were plated and treated with morphine (100 nM), morphine/naloxone (1 μM), morphine/ (+)naloxone (1 μM), morphine/LPS-RS (1, 10 and 100 ng ml^{-1}, Invitrogen), morphine/TNP-ATP (10 μM, Sigma), morphine/PPADS (pyridoxal-phosphate- 6-azophenyl-2′,4′-disulfonate, 10 μM, Sigma), morphine/TrkB-Fc (5 μg/ml, R&D Systems) or morphine/IgG-Fc (5 μg ml^{-1}, R&D Systems) once daily for 5 d. Control cultures were treated with either phosphate-buffered saline (PBS) or the above drugs in the absence of morphine once daily for 5 d.

microglia calcium imaging. Cells were incubated at 20–25 °C for 30 min with Fura-2 a.m. (2.5 μM, Molecular Probes) in ACSF containing 140 mM NaCl, 5.4 mM KCl, 1.3 mM $CaCl^2$, 10 mM HEPES and 33 mM glucose (pH 7.35, osmolarity 315–320 mOsm). ATP (50 μM, Sigma) was bath-applied. Excitation light was generated from a 75-W xenon arc lamp and passed alternatingly through 340- or 380-nm band-pass filters[56] (Omega Optical).

microglia whole-cell recording. ACSF was as above, except for 1 mM $MgCl_2$ and 2 mM $CaCl_2$. Pipettes contained 140 mM CsCl, 1 mM $MgCl_2$, 10 mM BAPTA, 10 mM HEPES, pH 7.2. ATP (50 μM) was applied for 2 s using a fast-step per- fusion system (SF-77B, Warner Instruments) and recorded using an Axopatch 1-D amplifier (Molecular Devices). The electrical signals were digitized with a DigiData 1200 (Molecular Devices) and filtered at 2 kHz.

Intrathecal injections of microglia. These experiments were performed as described previously[57]. Briefly, before intrathecal injection, microglia cultures were washed out in PBS, removed from the dish surface using a cell scraper and collected in 100 μl of PBS. Cell density was measured using a cell counter and the volume of PBS was adjusted to give a final density of 1,000 cells per 10 μl. This preparation was injected via lumbar puncture. Paw withdrawal threshold was tested before injection and after 1, 3 and 5 h. In a previous set of experiments with intrathecal catheter implants, we found that microglia produced a significant effect ($P < 0.01$) on withdrawal reflex only when administered dorsally, confirming a selective action at the SDH level (**Supplementary Fig. 3**).

Western blotting. Cultured microglia were harvested and collected in 100 μl of PBS containing a phosphatase inhibitor cocktail (2%, Sigma) and a broad spectrum protease inhibitor (2%, Sigma). After centrifugation, the pellet was resuspended in 3% sodium dodecyl sulfate (SDS, vol/vol) containing 15%

glycerol (vol/vol) and 75 mM Tris-base. Total protein was measured using a BCA protein assay reagent kit (Pierce). Samples were heated at 95 °C for 10 min in 2× sample buffer (Pierce), electrophoresed on a precast SDS polyacrylamide gradient gel (4–12% Tris-HCl, Bio-Rad) and transferred onto a nitrocellulose membrane. After blocking, membranes were incubated with rabbit antibody to P2X4R (1:1,000, Alomone, #- APR-002) or mouse antibody to actin (1:5,000, Sigma ,#-A5316), followed by incubation with horseradish peroxidase (HRP)-conjugated secondary antibody (1:10,000, Bio-Rad, #-170-6515, #-170-6516), ECL detection (Amersham) and densitometric quantification (ImageJ, US National Institutes of Health). Rat spinal cords were rapidly dissected and frozen in liquid nitrogen. Spinal cord homogenates were separated on a precast SDS polyacrylamide gradi- ent gel (4–12% Tris-HCl, Bio-Rad) or 4–12% Tris glycine gel (Invitrogen) and transferred onto nitrocellulose membrane. P2X4R detection was performed as described above. For KCC2 detection, gel loading was done in a Laemmli sample buffer (Bio-Rad) containing 0.5% lithium dodecyl sulfate (wt/vol) to solubilize KCC2. Membranes were incubated in PBS/milk (pH 7.4) and incubated overnight with the polyclonal rabbit antibody to KCC2 (1:1,000, Millipore, #-07-432)[23] at 4 °C. Membranes were washed and incubated for 2 h at 20–25 °C in rabbit-specific secondary antibody then quantified by direct detection of secondary antibody fluorescence at 700 and 800 nm (Odyssey Licor) . The relative amount of mono- meric or oligomeric KCC2 was calculated as described[23]. Full-length blots are shown in **Supplementary Figure 4**.

Histological procedures. Rats or mice were anesthetized and perfused tran- scardially with 4% paraformaldehyde (wt/vol) in 0.1 M phosphate buffer (pH 7.4). Spinal cord sections were obtained as described[58]. Sections were incub- ated overnight at 4 °C in rabbit antibody to KCC2 (1:1,000), guinea pig antibody to μ-receptor antibody (1:5,000, Neuromics, #-GP10106), mouse OX-42 antibody to CD11b (1:500, Millipore #-CBL1512; 1:1,000, Serotec, #-MCA275R). After washing, sections were incubated at 20–25 °C in a solution containing appropri- ate fluorochrome-conjugated secondary antibodies. Images were obtained with an Olympus FV300-IX71 confocal microscope (Olympus America) for KCC2 staining or with a Leica TCS SP2 confocal microscope (Leica) for CD11b immuno- cytochemistry (ICC). Images of CD11b ICC from intrathecal saporin/saporin- Mac1 experiments were acquired with a fluorescence microscope (Olympus). Laminar boundaries were identified as described[58]. Quantification was per- formed using ImageJ for CD11b ICC and using locally designed software for KCC2 (MathWorks). β-galactosidase activity in *P2rx4*$^{-/-}$ mouse spinal cords was revealed by incubation with a solution of X-Gal (1 mg ml^{-1}), 5 mM potassium ferrycyanide, 2 mM $MgCl_2$, 0.2% Triton X-100 (vol/vol) in PBS overnight at 37 °C. X-gal staining was quantified using ImageJ. No staining was detected in wild-type mice.

ELISA. Recovery of BDNF released from microglia was achieved using a Microcon YM-10 centrifugal

filter device (Millipore). As described previously[22], measurement of microglial BDNF was performed using a specific ELISA kit (detection range: 7.8–500 pg ml^{-1}) with BDNF standards (7.82–500 pg ml^{-1}) and 100 µl of supernatant sample run in triplicate (Chemicon). Samples were washed and incubated with biotinylated mouse monoclonal antibody to BDNF (1:1,000, Chemicon, #-CYT306), incubated with streptavidin-HRP conjugate, treated with 3,3′,5,5′-tetramethylbenzidine substrate and read by a spectrophotometer plate reader (Molecular Devices) at 450 nm. Samples were considered BDNF positive if their signal was higher than the background signal and was in the range of the standard curve. Data were normalized to the control.

Statistics. All data are given as the mean ± s.e.m. As data distributions were poorly fit by a Gaussian distribution, non-parametric tests were used (unless otherwise stated). Differences between groups were tested by Mann-Whitney test or by Kruskal-Wallis test with *post hoc* Dunn test. Repeated measures were analyzed by Friedmann test with *post hoc* Dunnet test or Wilcoxon test. Fisher's exact test was used for contingency tables. Bi-exponential fittings were compared by F test. Sample sizes are consistent with those reported in similar studies. Differences were considered to be significant at $P < 0.05$.

Acknowledgements

We thank K. Bachand for technical assistance with behavior, F. Rassendren (INSERM) for *P2rx4*$^{-/-}$mice, C.J. Evans (National Institute on Drug Abuse) for (+)naloxone and J. Vlahakis for (+)naloxone polarimetric analysis. This paper is dedicated to the memory of Karen Vandal, who passed away during the course of this study. This work was supported by Canadian Institutes for Health Research (CIHR) grants to Y.D.K., M.W.S., C.M.C. and J.-M.B., by the Krembil Foundation (Y.D.K. and M.W.S.), the Regione Piemonte/University of Turin Fellowship Program (F.F.), the CIHR Fellowship program (T.T. and L.-E.L.), the Howard Hughes Medical Institute (M.W.S.), the Anne and Max Tanenbaum Chair Program (M.W.S.), the Canada Research Chairs Program (C.M.C., J.-M.B. and M.W.S.), the Fonds de la recherche en santé du Québec Chercheur National Program (Y.D.K.) and the Ontario Research Fund Research Excellence Program (M.W.S.).

Author contributions

F.F., T.T., C.M.C., M.W.S. and Y.D.K. conceived and designed the project. C.M.C., J.-M.B., Y.D.K. and M.W.S. supervised the experiments. F.F., T.T., T.-A.M.M., S.L., T.D., L.-E.L., A.C., W.Z., D.M., S.B. and K.V. performed the experiments. N.D. performed computer simulations and contributed to interpretation of results. S.B. generated *CD11b-cre; Bdnf*$^{loxP/loxP}$ mice. F.F., T.T., T.-A.M.M., S.L., T.D., L.-E.L., A.C., N.D., W.Z. and A.G.G. analyzed the data. F.F., T.T., M.W.S. and

Y.D.K. wrote the manuscript. All of the authors read and discussed the manuscript.

Competing financial interests

The authors declare no competing financial interests.

1. Bekhit, M.H. Opioid-induced hyperalgesia and tolerance. *Am. J. Ther.* **17**, 498–510 (2010).
2. Lee, M., Silverman, S.M., Hansen, H., Patel, V.B. & Manchikanti, L. A comprehensive review of opioid-induced hyperalgesia. *Pain Physician* **14**, 145–161 (2011).
3. Mao, J., Sung, B., Ji, R.R. & Lim, G. Chronic morphine induces downregulation of spinal glutamate transporters: implications in morphine tolerance and abnormal pain sensitivity. *J. Neurosci.* **22**, 8312–8323 (2002).
4. Vanderah, T.W. *et al.* Tonic descending facilitation from the rostral ventromedial medulla mediates opioid-induced abnormal pain and antinociceptive tolerance. *J. Neurosci.* **21**, 279–286 (2001).
5. Heinke, B., Gingl, E. & Sandkuhler, J. Multiple targets of mu-opioid receptor–mediated presynaptic inhibition at primary afferent Adelta- and C-fibers. *J. Neurosci.* **31**, 1313–1322 (2011).
6. Zeng, J., Thomson, L.M., Aicher, S.A. & Terman, G.W. Primary afferent NMDA receptors increase dorsal horn excitation and mediate opiate tolerance in neonatal rats. *J. Neurosci.* **26**, 12033–12042 (2006).
7. Woolf, C.J. & Salter, M.W. Neuronal plasticity: increasing the gain in pain. *Science* **288**, 1765–1769 (2000).
8. Craig, A.D. Pain mechanisms: labeled lines versus convergence in central processing. *Annu. Rev. Neurosci.* **26**, 1–30 (2003).
9. Drdla, R., Gassner, M., Gingl, E. & Sandkuhler, J. Induction of synaptic long-term potentiation after opioid withdrawal. *Science* **325**, 207–210 (2009).
10. Sandkühler, J. Models and mechanisms of hyperalgesia and allodynia. *Physiol. Rev.* **89**, 707–758 (2009).
11. Zeilhofer, H.U., Benke, D. & Yevenes, G.E. Chronic pain states: pharmacological strategies to restore diminished inhibitory spinal pain control. *Annu. Rev. Pharmacol. Toxicol.* **52**, 111–133 (2012).
12. Coull, J.A. *et al.* Trans-synaptic shift in anion gradient in spinal lamina I neurons as a mechanism of neuropathic pain. *Nature* **424**, 938–942 (2003).
13. Keller, A.F., Beggs, S., Salter, M.W. & De Koninck, Y. Transformation of the output of spinal lamina I neurons after nerve injury and microglia stimulation underlying neuropathic pain. *Mol. Pain* **3**, 27 (2007).
14. Cordero-Erausquin, M., Coull, J.A., Boudreau, D., Rolland, M. & De Koninck, Y. Differential maturation of GABA action and anion reversal potential in spinal lamina I neurons: impact of chloride extrusion capacity. *J. Neurosci.* **25**, 9613–9623 (2005).
15. Sjøgren, P., Jonsson, T., Jensen, N.H., Drenck, N.E. & Jensen, T.S. Hyperalgesia and myoclonus in terminal cancer patients treated with continuous intravenous morphine. *Pain* **55**, 93–97 (1993).
16. Hewitt, S.A., Wamsteeker, J.I., Kurz, E.U. & Bains, J.S. Altered chloride homeostasis removes synaptic inhibitory constraint of the stress axis. *Nat. Neurosci.* **12**, 438–443 (2009).
17. Kemp, T., Spike, R.C., Watt, C. & Todd, A.J. The mu-opioid receptor (MOR1) is mainly restricted to neurons that do not contain GABA or glycine in the superficial dorsal horn of the rat spinal cord. *Neuroscience* **75**, 1231–1238 (1996).
18. Smirnov, S., Paalasmaa, P., Uusisaari, M., Voipio, J. & Kaila, K. Pharmacological isolation of the synaptic and nonsynaptic components of the GABA-mediated biphasic response in rat CA1 hippocampal pyramidal cells. *J. Neurosci.* **19**, 9252–9260 (1999).
19. Doyon, N. *et al.* Efficacy of synaptic inhibition depends on multiple, dynamically interacting mechanisms implicated in chloride homeostasis. *PLoS Comput. Biol.* **7**, e1002149 (2011).
20. Staley, K.J., Soldo, B.L. & Proctor, W.R. Ionic mechanisms of neuronal excitation by inhibitory $GABA_A$ receptors. *Science* **269**, 977–981 (1995).
21. Prescott, S.A., Sejnowski, T.J. & De Koninck, Y. Reduction of anion reversal potential subverts the inhibitory control of firing rate in spinal lamina I neurons: towards a biophysical basis for neuropathic pain. *Mol. Pain* **2**, 32 (2006).
22. Coull, J.A. *et al.* BDNF from microglia causes the shift in neuronal anion gradient underlying neuropathic pain. *Nature* **438**, 1017–1021 (2005).

23. Blaesse, P. *et al.* Oligomerization of KCC2 correlates with development of inhibitory neurotransmission. *J. Neurosci.* **26**, 10407–10419 (2006).
24. Chorin, E. *et al.* Upregulation of KCC2 activity by zinc-mediated neurotransmission via the mZnR/GPR39 receptor. *J. Neurosci.* **31**, 12916–12926 (2011).
25. Beggs, S. & Salter, M.W. Microglia-neuronal signalling in neuropathic pain hypersensitivity 2.0. *Curr. Opin. Neurobiol.* **20**, 474–480 (2010).
26. Zhao, P., Waxman, S.G. & Hains, B.C. Extracellular signal–regulated kinase-regulated microglia-neuron signaling by prostaglandin E2 contributes to pain after spinal cord injury. *J. Neurosci.* **27**, 2357–2368 (2007).
27. Tsuda, M. *et al.* P2X4 receptors induced in spinal microglia gate tactile allodynia after nerve injury. *Nature* **424**, 778–783 (2003).
28. Tsuda, M., Tozaki-Saitoh, H. & Inoue, K. Pain and purinergic signaling. *Brain Res. Rev.* **63**, 222–232 (2010).
29. Trang, T., Beggs, S., Wan, X. & Salter, M.W. P2X4 receptor–mediated synthesis and release of brain-derived neurotrophic factor in microglia is dependent on calcium and p38 mitogen–activated protein kinase activation. *J. Neurosci.* **29**, 3518–3528 (2009).
30. Ulmann, L. *et al.* Upregulation of P2X4 receptors in spinal microglia after peripheral nerve injury mediates BDNF release and neuropathic pain. *J. Neurosci.* **28**, 11263–11268 (2008).
31. De Koninck, Y. Altered chloride homeostasis in neurological disorders: a new target. *Curr. Opin. Pharmacol.* **7**, 93–99 (2007).
32. Mannion, R.J. *et al.* Neurotrophins: peripherally and centrally acting modulators of tactile stimulus-induced inflammatory pain hypersensitivity. *Proc. Natl. Acad. Sci. USA* **96**, 9385–9390 (1999).
33. Boillée, S. *et al.* Onset and progression in inherited ALS determined by motor neurons and microglia. *Science* **312**, 1389–1392 (2006).
34. Rios, M. *et al.* Conditional deletion of brain-derived neurotrophic factor in the postnatal brain leads to obesity and hyperactivity. *Mol. Endocrinol.* **15**, 1748–1757 (2001).
35. Matthes, H.W. *et al.* Loss of morphine-induced analgesia, reward effect and withdrawal symptoms in mice lacking the mu-opioid-receptor gene. *Nature* **383**, 819–823 (1996).
36. Horvath, R.J., Romero-Sandoval, E.A. & De Leo, J.A. Inhibition of microglial P2X4 receptors attenuates morphine tolerance, Iba1, GFAP and mu opioid receptor protein expression while enhancing perivascular microglial ED2. *Pain* **150**, 401–413 (2010).
37. Hutchinson, M.R. *et al.* Exploring the neuroimmunopharmacology of opioids: an integrative review of mechanisms of central immune signaling and their implications for opioid analgesia. *Pharmacol. Rev.* **63**, 772–810 (2011).
38. Xu, J., Xu, M., Rossi, G.C., Pasternak, G.W. & Pan, Y.X. Identification and characterization of seven new exon 11–associated splice variants of the rat mu opioid receptor gene, *OPRM1*. *Mol. Pain* **7**, 9 (2011).
39. Wang, X. *et al.* Morphine activates neuroinflammation in a manner parallel to endotoxin. *Proc. Natl. Acad. Sci. USA* **109**, 6325–6330 (2012).
40. Bohn, L.M., Gainetdinov, R.R., Lin, F.T., Lefkowitz, R.J. & Caron, M.G. Mu-opioid receptor desensitization by beta-arrestin-2 determines morphine tolerance, but not dependence. *Nature* **408**, 720–723 (2000).
41. Mao, J. Opioid-induced abnormal pain sensitivity: implications in clinical opioid therapy. *Pain* **100**, 213–217 (2002).
42. Wang, Y. *et al.* Blockade of PDGFR-beta activation eliminates morphine analgesic tolerance. *Nat. Med.* **18**, 385–387 (2012).
43. Knabl, J. *et al.* Reversal of pathological pain through specific spinal GABAA receptor subtypes. *Nature* **451**, 330–334 (2008).
44. Asiedu, M., Ossipov, M.H., Kaila, K. & Price, T.J. Acetazolamide and midazolam act synergistically to inhibit neuropathic pain. *Pain* **148**, 302–308 (2010).
45. Horvath, R.J. & DeLeo, J.A. Morphine enhances microglial migration through modulation of P2X4 receptor signaling. *J. Neurosci.* **29**, 998–1005 (2009).
46. Takayama, N. & Ueda, H. Morphine-induced chemotaxis and brain-derived neurotrophic factor expression in microglia. *J. Neurosci.* **25**, 430–435 (2005).
47. Merighi, A. *et al.* BDNF as a pain modulator. *Prog. Neurobiol.* **85**, 297–317 (2008).
48. Zhao, J. *et al.* Nociceptor-derived brain-derived neurotrophic factor regulates acute and inflammatory, but not neuropathic pain. *Mol. Cell. Neurosci.* **31**, 539–548 (2006).

49. Boulenguez, P. *et al.* Down-regulation of the potassium-chloride cotransporter KCC2 contributes to spasticity after spinal cord injury. *Nat. Med.* **16**, 302–307 (2010).
50. Vargas-Perez, H. *et al.* Ventral tegmental area BDNF induces an opiate-dependent-like reward state in naive rats. *Science* **324**, 1732–1734 (2009).
51. Sim, J.A. *et al.* Altered hippocampal synaptic potentiation in P2X4 knock-out mice. *J. Neurosci.* **26**, 9006–9009 (2006).
52. Poltorak, A. *et al.* Defective LPS signaling in C3H/HeJ and C57BL/10ScCr mice: mutations in *Tlr4* gene. *Science* **282**, 2085–2088 (1998).
53. Wang, Y. *et al.* Age-dependent morphine tolerance development in the rat. *Anesth. Analg.* **100**, 1733–1739 (2005).
54. Trang, T., Ma, W., Chabot, J.G., Quirion, R. & Jhamandas, K. Spinal modulation of calcitonin gene–related peptide by endocannabinoids in the development of opioid physical dependence. *Pain* **126**, 256–271 (2006).
55. Yaksh, T.L., Jessell, T.M., Gamse, R., Mudge, A.W. & Leeman, S.E. Intrathecal morphine inhibits substance P release from mammalian spinal cord *in vivo*. *Nature* **286**, 155–157 (1980).
56. Salter, M.W. & Hicks, J.L. ATP causes release of intracellular Ca^{2+} via the phospholipase C beta/IP3 pathway in astrocytes from the dorsal spinal cord. *J. Neurosci.* **15**, 2961–2971 (1995).
57. De la Calle, J.L. & Paino, C.L. A procedure for direct lumbar puncture in rats. *Brain Res. Bull.* **59**, 245–250 (2002).
58. Lorenzo, L.E., Ramien, M., St Louis, M., De Koninck, Y. & Ribeiro-da-Silva, A. Postnatal changes in the Rexed lamination and markers of nociceptive afferents in the superficial dorsal horn of the rat. *J. Comp. Neurol.* **508**, 592–604 (2008).

Figure 1: Repeated morphine administration causes hyperalgesia and tolerance.

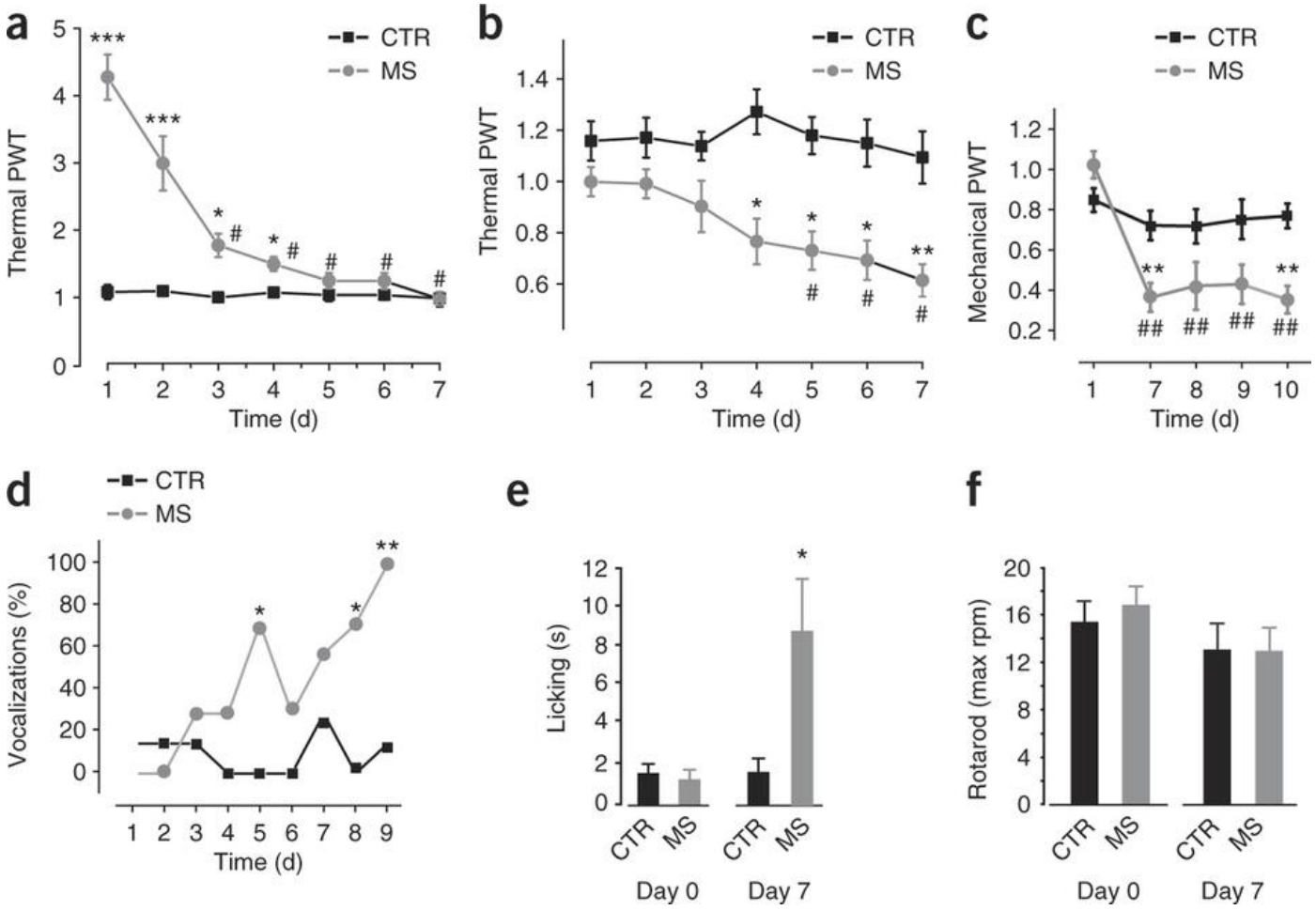

Figure 1 Repeated morphine administration causes hyperalgesia and tolerance. (**a**–**c**) Time course of morphine tolerance and pain hypersensitivity assessed by Hargreaves plantar test and von Frey filament in rats. (**a**) Thermal pain threshold 1 h after morphine (days 3–7 versus day 1, $\chi^2 = 61.5$, $^{\#}P < 0.001$) or saline injection (morphine versus saline at days 1–4, $^{*}P < 0.05$, $^{***}P < 0.001$). CTR, saline control; MS, morphine sulfate; PWT, paw withdrawal threshold. (**b**) Thermal pain threshold before morphine (days 5–7 versus day 1, $\chi^2 = 20.7$, $^{\#}P < 0.001$) and saline injection (morphine versus saline at days 4–7, $^{*}P < 0.05$, $^{**}P < 0.01$). (**c**) Mechanical pain threshold before morphine or saline injection. At day 7, the threshold of morphine-treated rats ($n = 7$) was significantly reduced as compared with the threshold at day 1 ($\chi^2 = 13.58$, $^{\#}P < 0.01$) and the saline group ($n = 6$, $^{**}P < 0.01$). (**d**,**e**) Progressive increase in nociceptive behaviors in morphine-treated rats as compared with saline-treated controls. (**d**) Percentage of vocalizing rats during subcutaneous injections (day 5–9 versus day 1, $^{*}P < 0.05$, $^{**}P < 0.01$). (**e**) Licking time after thermal stimulation (day 0, $P > 0.05$; day 7, U = 7, $^{*}P < 0.05$). (**f**) Maximal running speed at day 0 and day 7 of saline or morphine injections assessed by rotarod before the morning injection (U = 21, $P > 0.05$). All threshold values were normalized to the baseline. Error bars in all panels represent s.e.m.

Figure 2: Morphine disrupts Cl^- homeostasis in lamina I neurons.

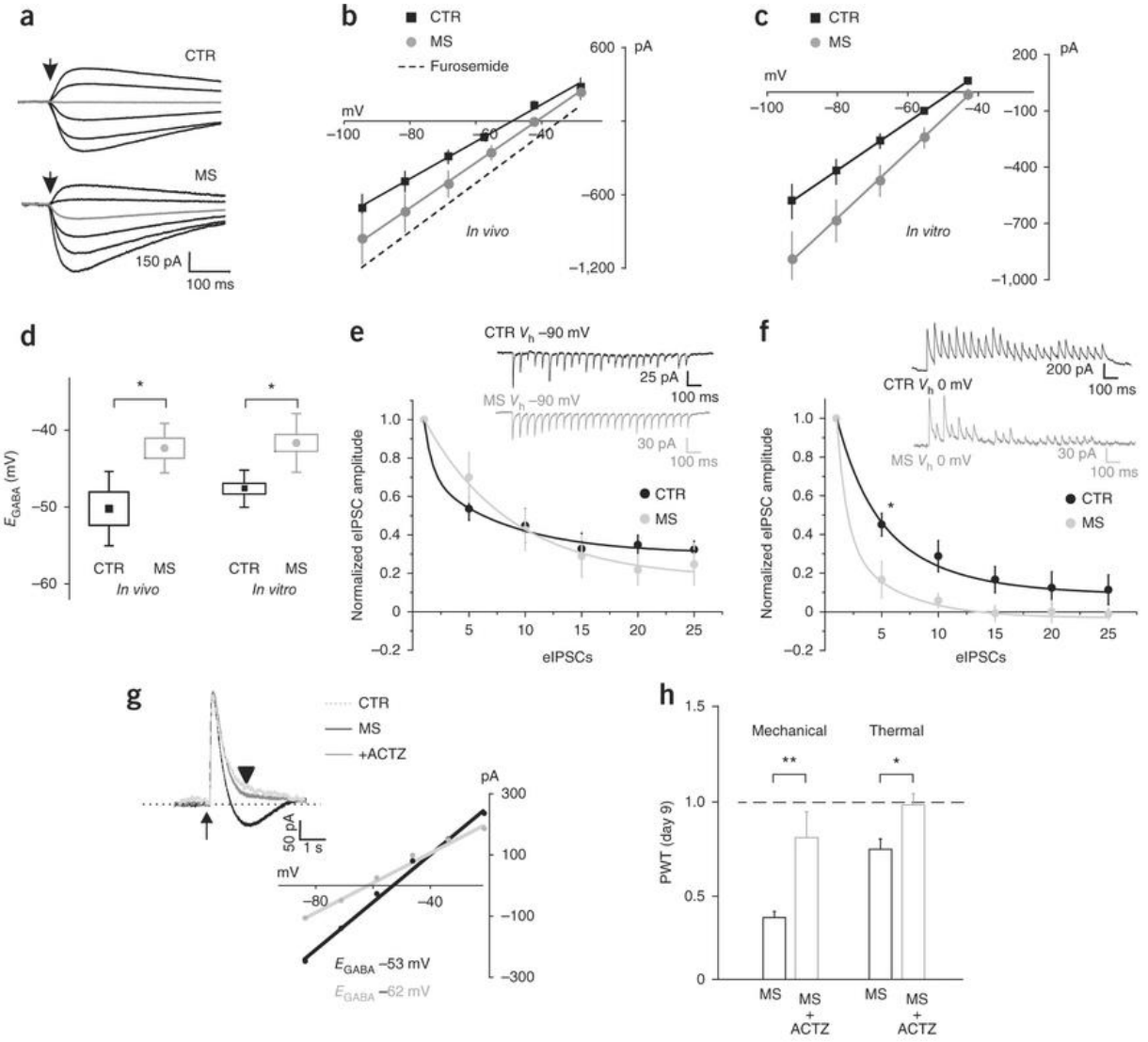

Figure 2 Morphine disrupts Cl^- homeostasis in lamina I neurons. (**a**,**b**) Decrease in Cl^- extrusion capacity in lamina I neurons after *in vivo* morphine treatments in rats. (**a**) Responses to 30-ms GABA puffs following saline or morphine treatments in the presence of a Cl^- load (29 mM). The response obtained at –55.5 mV is shown in gray. (**b**) *I-V* relationships for $GABA_A$ currents obtained from morphine-treated rats (n = 6 cells) is right-shifted as compared with controls (n = 5 cells). The dashed line indicates the *I-V* relationship when Cl^- extrusion capacity was blocked by the KCC2 antagonist furosemide. (**c**) Effect of *in vitro* morphine (1 µM, >3 h, n = 7 cells) on *I-V* relationships for $GABA_A$ currents versus saline control (n = 6 cells). (**d**) Pooled E_{GABA} of neurons shown in **b** (U = 2) and **c** (U = 6, $^*P < 0.05$). (**e**,**f**) Cl^- accumulation under repetitive inhibitory input. (**e**) Representative traces (average of ten repetitions) from a control (black) and an *in vitro* morphine-treated lamina I neuron (gray) clamped at –90 mV (top). The rate of eIPSC amplitude depression during repetitive stimulation (20 Hz) is shown below. Amplitude values were normalized to the first eISPC. No differences were observed (CTR, n = 6 cells; MS, n = 4 cells; F = 0.8, $P > 0.05$). (**f**) Data are presented as in **e** for a neuron clamped at 0 mV. Note the larger and faster eIPSC depression in morphine-treated neurons. Differences between morphine and controls were significant (CTR, n = 6; MS, n = 4 cells; F = 21.98). (**g**) Gramicidin-perforated patch-clamp recording of GABA responses obtained at –60 mV in control (red dotted line) and from a morphine treated lamina I neuron before (black) and after ACTZ (50 µM, gray) Traces are scaled to the peak amplitude; arrow indicates the GABA puff. Note the biphasic response in the morphine neuron and the monophasic response following ACTZ. Below, *I-V* curves measured 1 s after the pulse (black arrowhead). Note the increased E_{GABA} difference before and after ACTZ. (**h**) Effect of intrathecal ACTZ (22.5 µg, day 7–9) on morphine-induced mechanical (saline, n = 5; ACTZ, n = 5; U = 0, $^{**}P < 0.01$) and thermal (saline, n = 11; ACTZ, n = 9; U = 15.5) pain hypersensitivity in rats. All threshold values were normalized to the baseline. The dashed line represents the baseline threshold. Error bars in all panels represent s.e.m.

Figure 3: Morphine effects on activity and expression of KCC2.

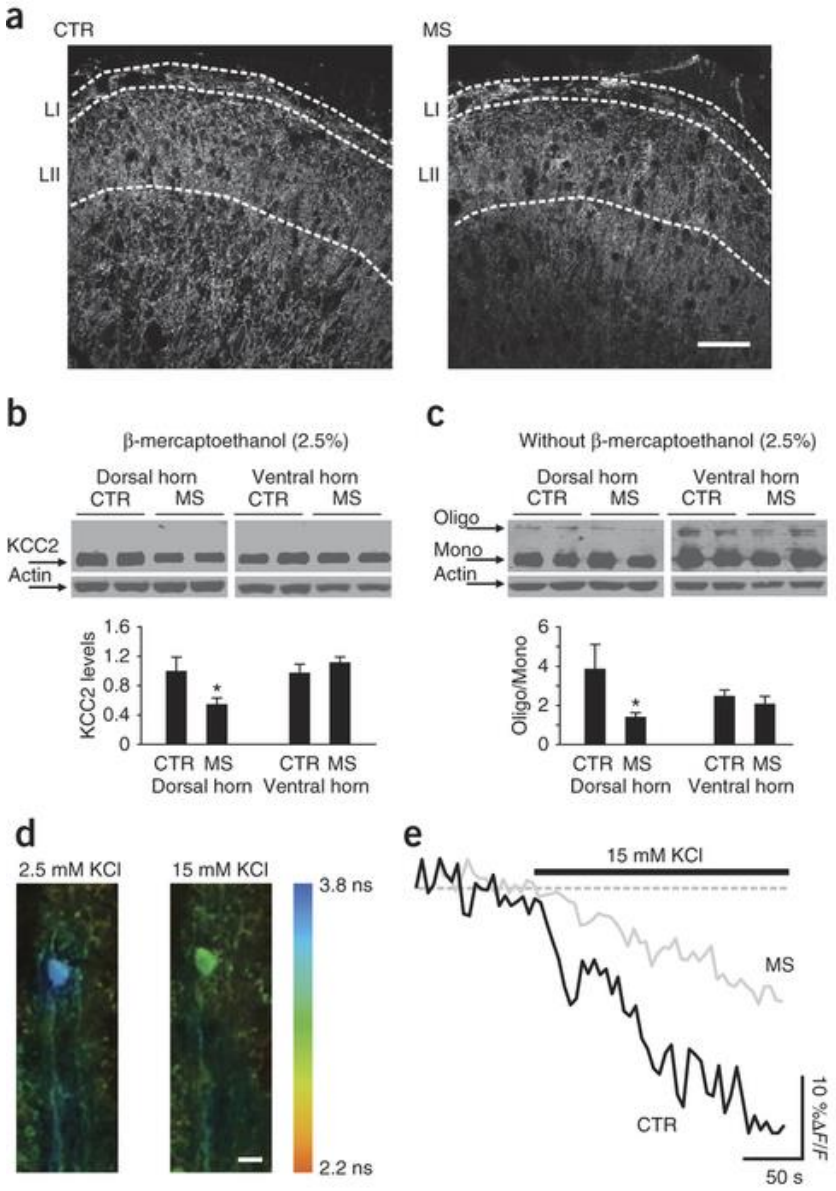

Figure 3 Morphine effects on activity and expression of KCC2. (**a**) KCC2 immunostaining in rat lamina I and lamina II following 7 d of saline or morphine injections. Scale bar represents 50 µm. (**b**) Western blot showing the total KCC2 expression in the dorsal and ventral horn from saline- and morphine-treated rats. Histograms show quantification of KCC2 expression normalized to the actin level in the dorsal (one-tail *t* test, $t = 2.1$, $^*P < 0.05$) and ventral horn (one-tail *t* test, $t = –1.1$, $P > 0.05$). (**c**) Western blot performed without β-mercaptoethanol to preserve KCC2 oligomerization. The histograms show quantification of KCC2 oligmer/monomer ratio in the dorsal ($n = 8$ control rats, $n = 9$ morphine-treated rats, one-tail *t* test, $t = 2.1$, $P < 0.05$) and the ventral horn (one-tail *t* test, $t = 0.6$, $P > 0.05$). (**d**,**e**) Chloride imaging from rat spinal cord slices loaded with the Cl^- -sensitive dye MQAE. (**d**) Pseudocolor images showing lifetime maps from a control lamina I neuron in the presence of 2.5 or 15 mM KCl. Lifetimes from lamina I neurons in control conditions (3.44 ± 0.34 ns, $n = 11$ cells) were significantly shortened (reflecting quenching of MQAE fluorescence) 15 min after exposure to high extracellular KCl to reverse KCC2 transport (3.02 ± 0.24 ns, $n = 11$, $P < 0.001$). (**e**) Representative traces of fluorescence intensity in control (black) and morphine-treated neuron (gray) showing the rate of intracellular Cl^- accumulation ($\%\Delta F/F_0$) in the presence of 15 mM KCl. Steady-state lifetime measurements just before 15 mM KCl solutions were not different (control, 3.37 ± 0.06 ns, 7.0 ± 0.7 mM Cl^{-1}; morphine, 3.23 ± 0.06 ns, 8.6 ± 0.8 mM Cl^- ; U = 38, $P > 0.05$). Error bars in all panels represent s.e.m.

Figure 4: Morphine-induced hyperalgesia depends on microglia activation.

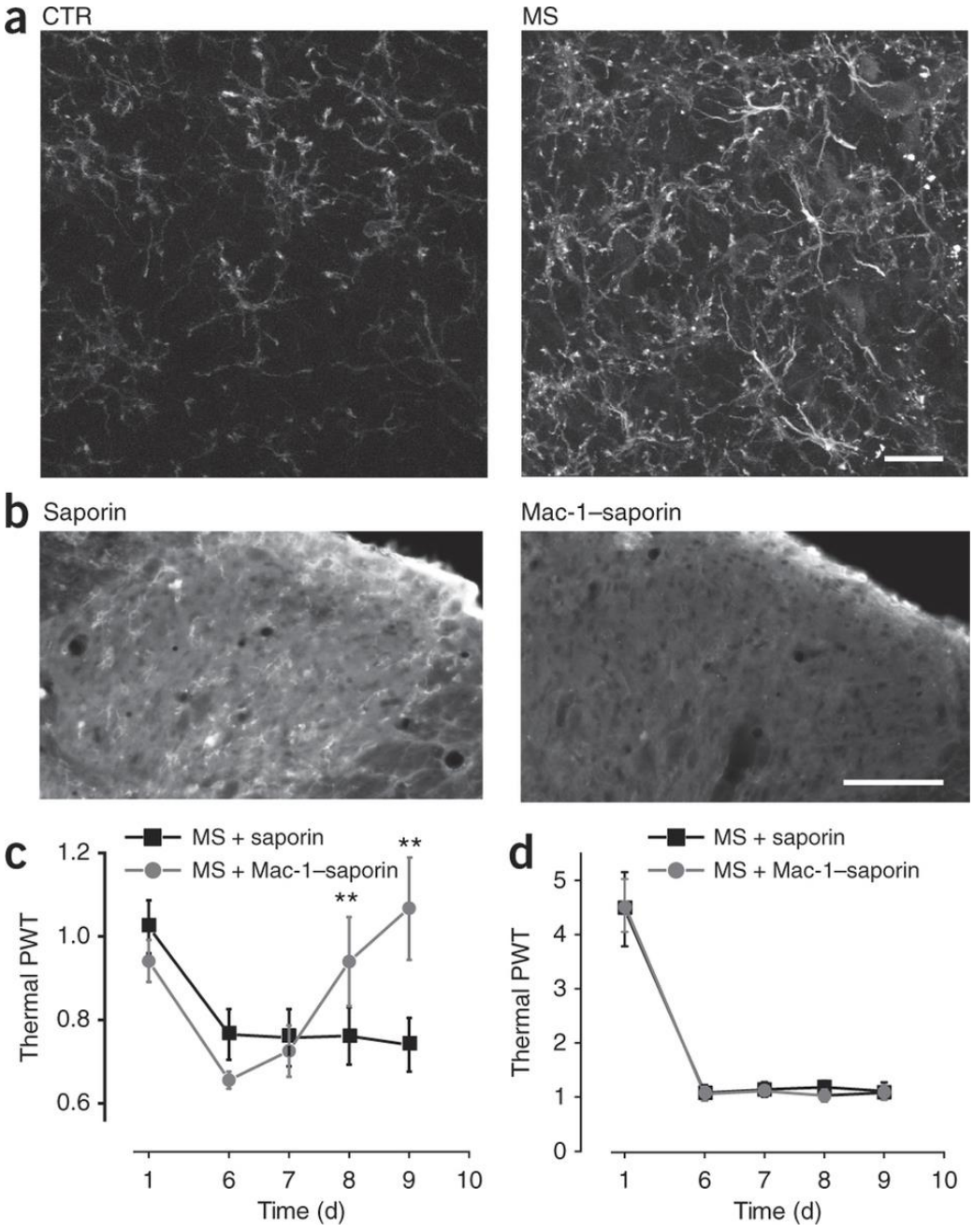

Figure 4 Morphine-induced hyperalgesia depends on microglia activation. (**a**) CD11b expression in rat SDH following 5 d of saline or morphine treatment (scale bar represents 30 µm) and fluorescence intensity quantification (CTR, 0.84 ± 0.06 i.u., n = 28 sections; MS, 2.78 ± 0.22 i.u., n = 34 sections; U = 8, $P < 0.001$). (**b**–**d**) Effects of intrathecal injection of saporin-conjugated antibody to Mac-1 (Mac-1–saporin; versus saporin alone) on SDH CD11b expression, morphine-induced hyperalgesia and tolerance (intrathecal injections were performed from day 7 to 9 of morphine treatment). (**b**) CD11b expression in SDH after microglia depletion with antibody to Mac1 (saporin, 10.12 ± 1.32 i.u., n = 17 sections; Mac-1–saporin, 7.84 ± 2.23 i.u., n = 16 sections; U = 55, $^{**}P < 0.01$). Scale bar represents 50 µm. (**c**) Thermal pain threshold before morphine injection (Mac-1–saporin versus saporin alone at day 9, U = 1, $^{**}P < 0.01$). (**d**) Thermal pain threshold 1 h after morphine injection (day 9, U = 12, $P > 0.05$). All threshold values were normalized to the baseline. Error bars in all panels represent s.e.m.

Figure 5: P2X4Rs in microglia are required for morphine-induced hyperalgesia.

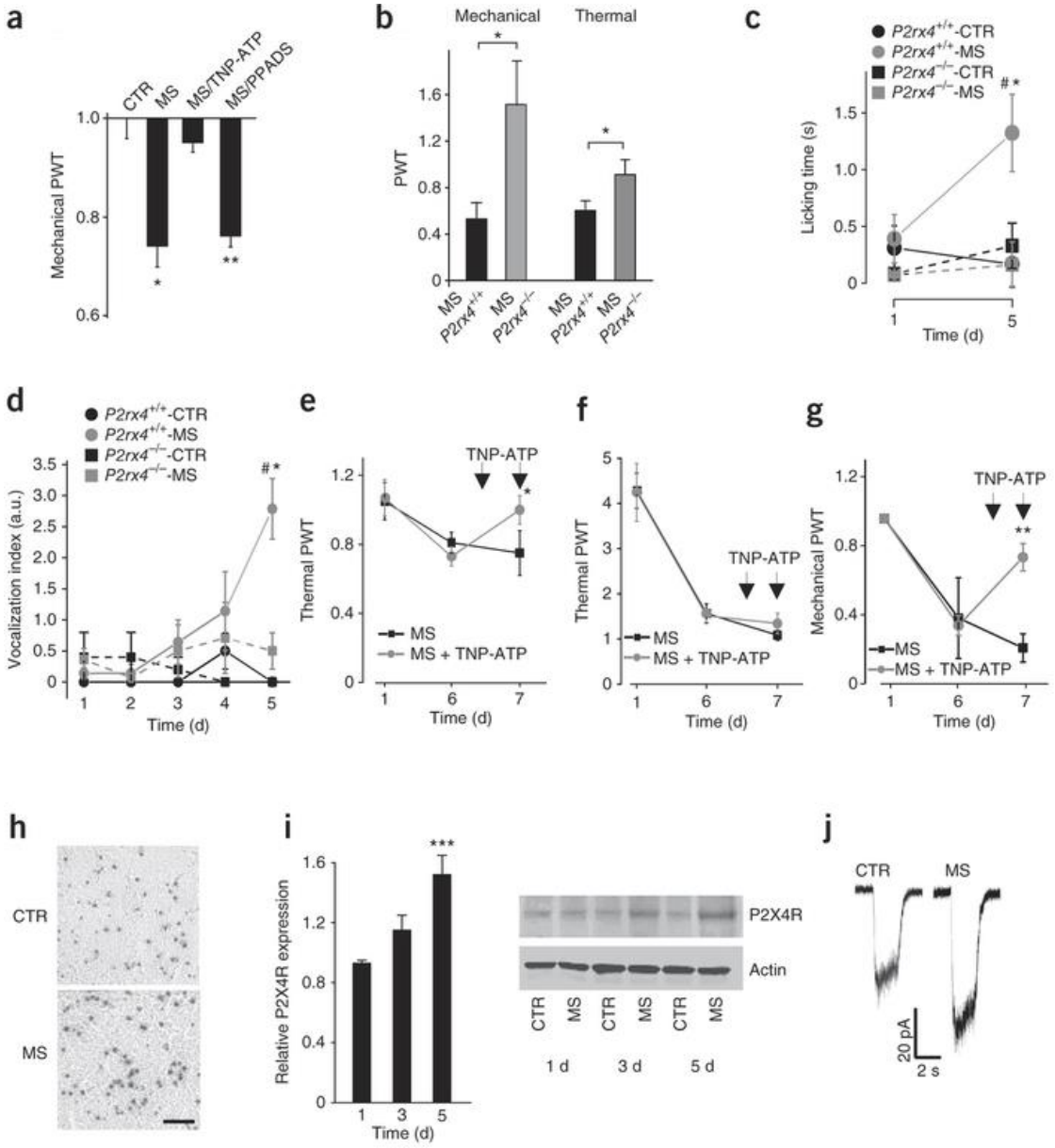

Figure 5 P2X4Rs in microglia are required for morphine-induced hyperalgesia. (**a**) Rat mechanical pain threshold 5 h after intrathecal injections of cultured microglia treated with morphine (100 nM, $n = 7$, H = 19.98, $*P < 0.01$), morphine + TNP-ATP ($n = 5$, $P > 0.05$), morphine + PPADS ($n = 8$, $**P < 0.01$), versus CTR ($n = 7$). (**b**–**d**) Lack of hyperalgesia in *P2rx4*$^{-/-}$ mice. (**b**) Thermal ($n = 5$ mice per group) and mechanical ($n = 7$ mice per group) pain threshold after 5 d of subcutaneous morphine injections in *P2rx4*$^{+/+}$ mice and *P2rx4*$^{-/-}$ mice (mechanical, U = 5; thermal, U = 2; $*P < 0.05$). (**c**) Licking time following mechanical stimulation of the paw (morphine-treated *P2rx4*$^{+/+}$ versus morphine-treated *P2rx4*$^{-/-}$, $*P < 0.05$; # significant differences **[AU: *P* value?]** compared with the baseline, $P < 0.05$). (**d**) Vocalizations produced by subcutaneous injections (morphine-treated *P2rx4*$^{+/+}$ versus other groups, $*P < 0.05$; # significant differences compared with the baseline, $P < 0.05$). (**e**–**g**) Effect of intrathecal TNP-ATP (30 nmol) on MIH in rats. (**e**) Thermal pain threshold before morphine injection in vehicle ($n = 8$) versus TNP-ATP–injected rats ($n = 8$, day 7, U = 13, $*P < 0.05$). (**f**) Thermal pain threshold 1 h after morphine. (**g**) Mechanical withdrawal threshold following TNP-ATP in morphine-treated rats measured before morphine injection (day 7; CTR, $n = 6$; TNP-ATP, $n = 7$; U = 0, $**P < 0.01$). (**h**) X-gal staining in *P2rx4*$^{-/-}$ mice. The percentage SDH staining area of control (3.6 ± 0.3%, $n = 5$ sections) and morphine-treated mice (4.8 ± 0.3%, $n = 12$ sections, U = 10, $*P < 0.05$). Scale bar represents 30 µm. (**i**,**j**) Increased expression and function of P2X4R in morphine-treated (100 nM) microglia cultures. (**i**) Expression of P2X4R after morphine treatment normalized to the saline controls for 1 d ($n = 7$ trials), 3 d ($n = 7$) and 5 d ($n = 7$, H = 19.35, $***P < 0.001$). (**j**) ATP-mediated currents in morphine-treated microglia over 5 d (peak current normalized to the pre-ATP baseline, 1.6 ± 0.2; $n = 12$ cells, U = 91, $*P < 0.05$) versus control (1.0 ± 0.1, $n = 28$ cells). All threshold values in the figure are normalized to the baseline. Error bars in all panels represent s.e.m.

Figure 6 Altered Cl^- homeostasis in spinal neurons and morphine-induced hyperalgesia are dependent on P2X4R-BDNF-TrkB signaling.

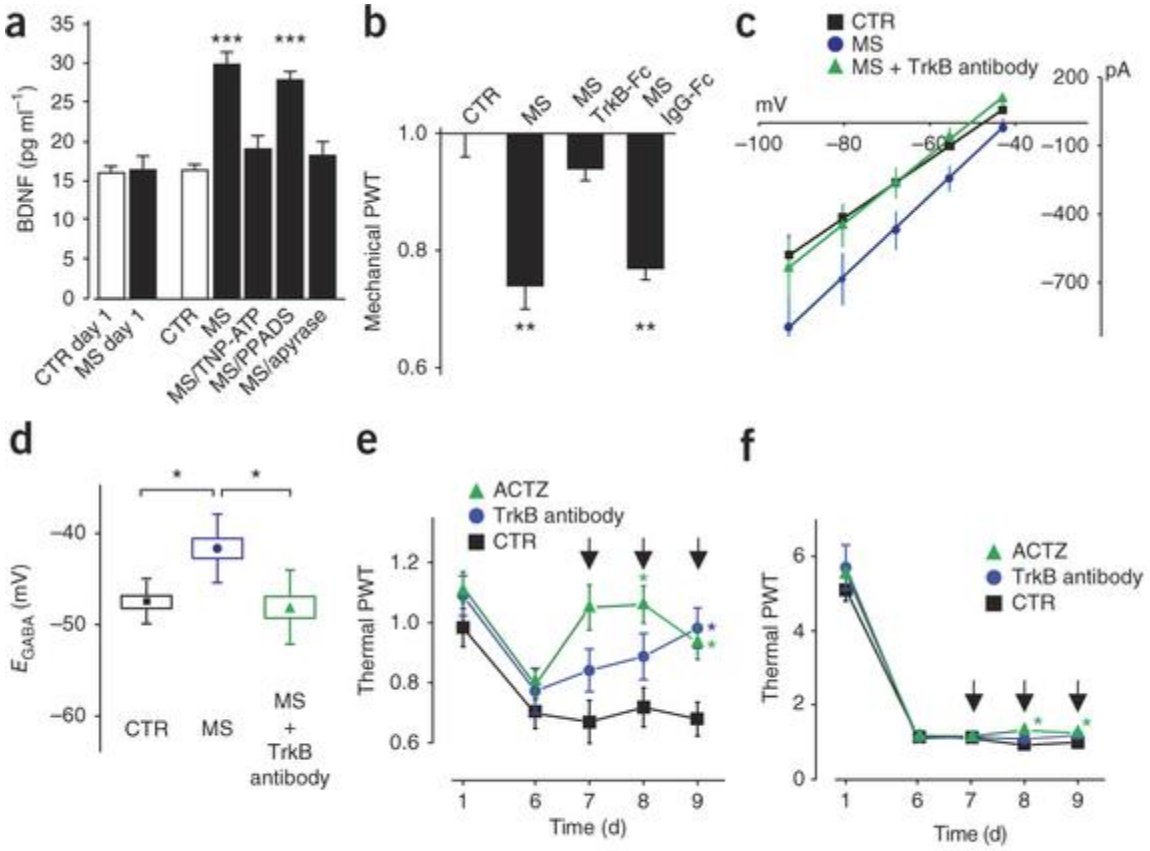

Figure 6 Altered Cl^- homeostasis in spinal neurons and morphine-induced hyperalgesia are dependent on P2X4R-BDNF-TrkB signaling. (**a**) Enzyme-linked immunosorbent assay (ELISA)-based measurement of BDNF release from cultured microglia treated with 100 nM morphine (n = 14 trials, H = 30.17, ***P < 0.001), morphine + TNP-ATP (n = 5, P > 0.05), morphine + PPADS (n = 5), morphine + apyrase (n = 5, P > 0.05) or saline (n = 14). (**b**) Rat mechanical withdrawal threshold 5 h after intrathecal injection of morphine-treated microglia (n = 7, H = 23.66, **P < 0.01), morphine + TrkB-Fc (n = 7, P > 0.05), morphine + IgG-Fc (n = 7) or saline (n = 7). (**c**,**d**) Effect of antibody to TrkB (1 μg ml^{-1}) on morphine-induced shift of E_{GABA} in lamina I neurons *in vitro*. Shown are *I-V* relationships for $GABA_A$ currents after incubation with morphine (n = 12 cells) or morphine + antibody to TrkB (n = 7) or in control (n = 6) (**c**) and the respective E_{GABA} values (H = 11.16, *P < 0.05; **d**). (**e**,**f**) Effect of intrathecal injections in rats of ACTZ and antibody to TrkB on morphine-induced pain hypersensitivity and tolerance by Hargreaves plantar test. (**e**) Thermal withdrawal threshold before morphine in ACTZ-treated (22.5 μg, n = 9), antibody to TrkB–treated (30 μg, n = 7) and vehicle-injected rats (n = 11, day 9; arrows indicate injections). (**f**) Thermal pain threshold 1 h after morphine treatment in ACTZ-, TrkB antibody– and vehicle-injected groups (ACTZ versus control group at days 8–9; arrows indicate injections). All threshold values were normalized to the baseline. Error bars in all panels represent s.e.m.

Figure 7: Genetic deletion of *Bdnf* from microglia abrogates development of morphine-induced hyperalgesia, but not tolerance.

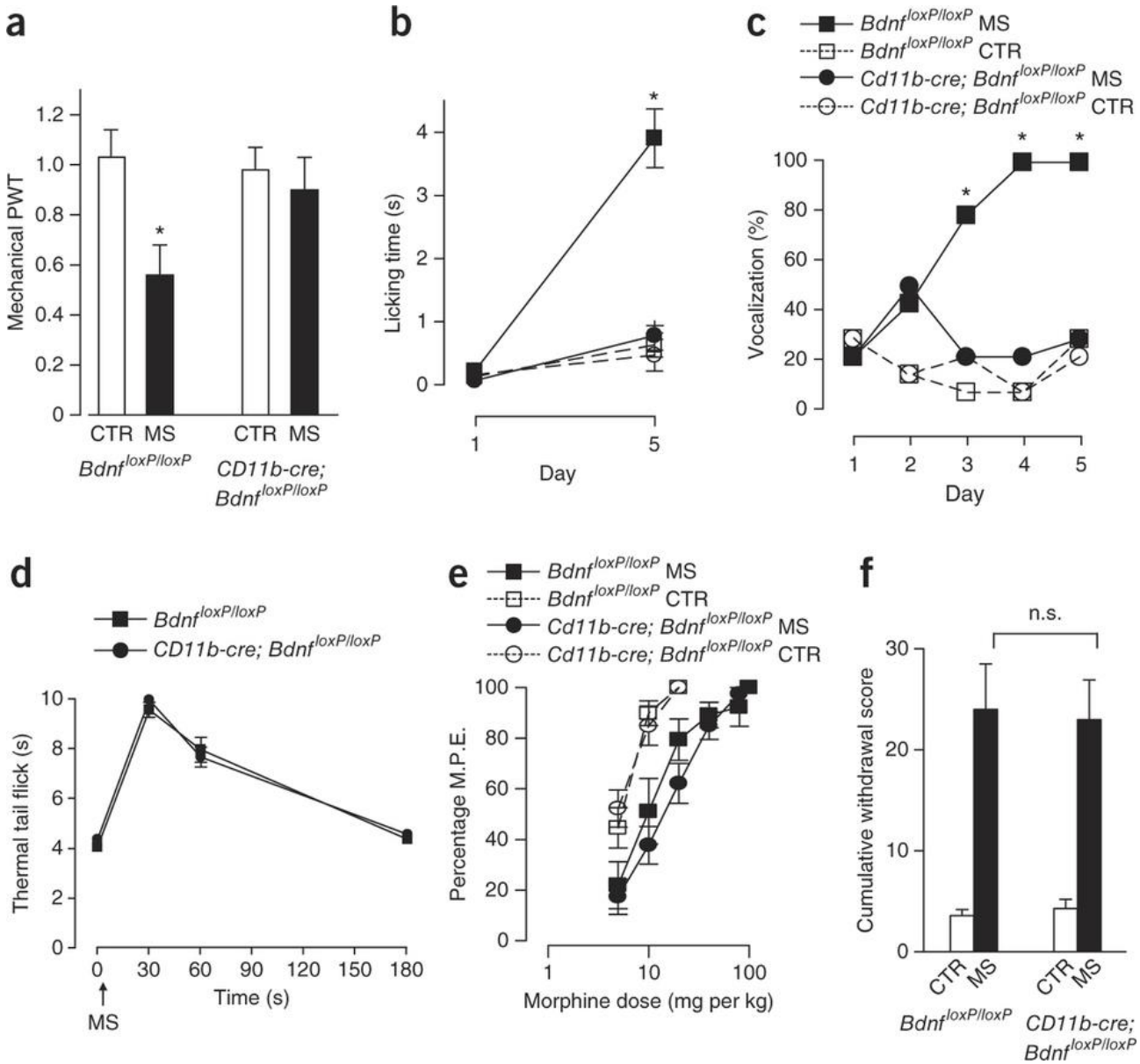

Figure 7 Genetic deletion of *Bdnf* from microglia abrogates development of morphine-induced hyperalgesia, but not tolerance. (**a**–**c**) Assessment of morphine-induced hyperalgesia in *CD11b-cre; Bdnf$^{loxP/loxP}$* mice (n = 7 mice) and *Bdnf$^{loxP/loxP}$* mice (n = 7). (**a**) Effect of 5 d of morphine on mechanical threshold (F = 3.499). (**b**) Licking time following mechanical stimulation of the hindpaw (H = 16.21). (**c**) Vocalizations produced by subcutaneous injections. Legend in inset applies to **b** and **c**. (**d**,**e**) Assessment of morphine antinociception in *CD11b-cre; Bdnf$^{loxP/loxP}$* mice (n = 7) and *Bdnf$^{loxP/loxP}$* mice (n = 7). (**d**) Time course of antinociceptive response to a single dose of morphine in morphine-naive mice. (**e**) Morphine dose-response curves following 5 d of morphine or saline injections in *CD11b-cre; Bdnf$^{loxP/loxP}$* mice (n = 7) and *Bdnf$^{loxP/loxP}$* mice (n = 7). The rightward shift in morphine-treated mice indicates the development of morphine tolerance in both *CD11b-cre; Bdnf$^{loxP/loxP}$* and *Bdnf$^{loxP/loxP}$* mice, with no significant differences between the two genotypes (ED50 of saline-injected controls: *Bdnf$^{loxP/loxP}$*, 3.5 ± 0.3 mg per kg; *CD11b-cre; Bdnf$^{loxP/loxP}$*, 3.3 ± 0.3 mg per kg; $P > 0.05$; morphine treated: *Bdnf$^{loxP/loxP}$*, 16.5 ± 1.0 mg per kg; *CD11b-cre; Bdnf$^{loxP/loxP}$*, 14.3 ± 1.1 mg per kg; $P > 0.05$). (**f**) Naloxone-precipitated withdrawal syndrome in *CD11b-cre; Bdnf$^{loxP/loxP}$* mice (CTR, n = 3; MS, n = 6) and *Bdnf$^{loxP/loxP}$* mice (CTR, n = 5; MS, n = 5). Withdrawal cumulative score was significantly higher in both morphine-treated groups as compared with the saline controls, but no differences were detected between *CD11b-cre; Bdnf$^{loxP/loxP}$* and *Bdnf$^{loxP/loxP}$* mice (F = 10.20, $P < 0.01$). n.s., not significant ($P > 0.05$; *$P < 0.05$). All threshold values were normalized to the baseline. Error bars in all panels represent s.e.m.

Figure 8: Activation of two separate signaling pathways is necessary for morphine-induced hyperalgesia.

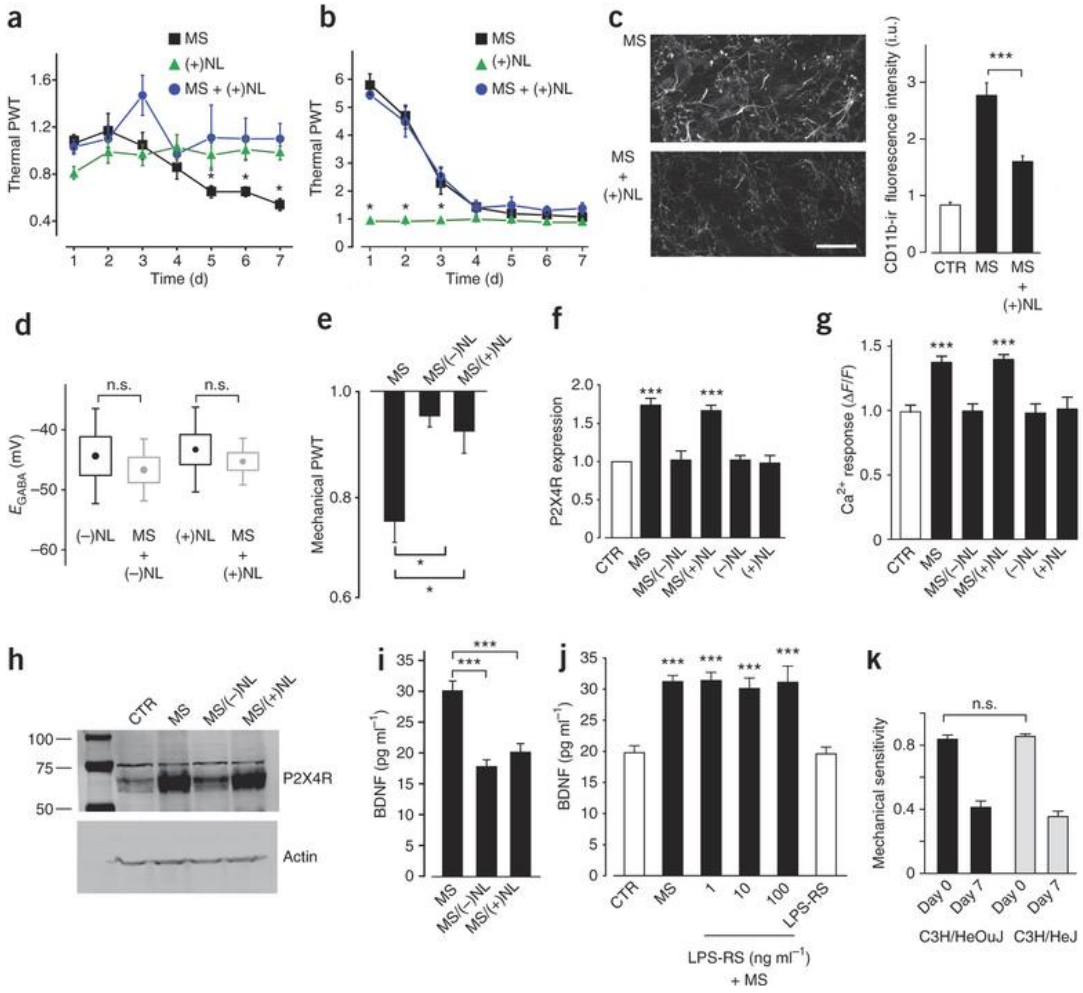

Figure 8: Activation of two separate signaling pathways is necessary for morphine-induced hyperalgesia. (**a**–**c**) Effect of intrathecal injections of low doses of (+)naloxone (5 ng, (+)NL) on morphine-induced pain hypersensitivity, tolerance and microglia activation. (**a**) Thermal withdrawal threshold before morphine or saline injections in (+)naloxone- or vehicle-treated rats ((+)naloxone, n = 8; morphine + (+)naloxone, n = 7; morphine, n = 8). (**b**) Thermal pain threshold 1 h after treatment. (**c**) CD11b immunostaining in rat SDH following 5 d of intrathecal morphine or morphine and (+)naloxone and quantification (CTR, n = 28 sections; MS, n = 34 sections; morphine + (+)naloxone, n = 34 sections). Scale bar represents 30 μm. (**d**) Lamina I E_{GABA} following 3 h *in vitro* with (−)naloxone alone (n = 6 cells) versus morphine and (−)naloxone (n = 6, U = 14, P > 0.05), and with (+)naloxone (n = 6) versus morphine and (+)naloxone (n = 8, U = 26, P > 0.05). (**e**) Mechanical withdrawal threshold 5 h after intrathecal injections of microglia cultures treated with morphine and (−)naloxone (n = 8, H = 12.97), morphine and (+)naloxone (n = 5), or morphine alone (n = 7). (**f**) Western blot analysis of P2X4R protein expression in microglia cultures following treatment with morphine (100 nM, n = 10 trials, H = 26.49), morphine and (−)naloxone (P > 0.05), morphine and (+)naloxone (n = 5), (−)naloxone (n = 3, P > 0.05), (+)naloxone (n = 6, P > 0.05), or saline (n = 10). (**g**) ATP-evoked rise in intracellular [Ca^{2+}] in cultured microglia treated with morphine (100 nM, n = 54 cells, H = 67.98), morphine and (−)naloxone (n = 38, P > 0.05), morphine and (+)naloxone (n = 40), (−)naloxone (n = 15, P > 0.05), (+)naloxone (n = 15, P > 0.05), or saline (n = 35). (**h**) Western blot of P2X4R protein from spinal cords isolated from rats treated for 5 d with intrathecal saline, morphine, morphine and (−)naloxone, or morphine and (+)naloxone. (**i**) ELISA-based measurement of BDNF release from microglia treated with morphine and (−)naloxone (n = 5 trials, H = 14.29), morphine and (+)naloxone (n = 5), or morphine (n = 14). (**j**) ELISA-based measurement of BDNF release from microglia treated with morphine (n = 4 trials, H = 15.84), morphine and 1 ng ml^{-1} LPS-RS 1 (n = 4), morphine and 10 ng ml^{-1} LPS-RS (n = 4), morphine and 100 ng ml^{-1} LPS-RS (n = 4), 100 ng ml^{-1} LPS-RS (n = 4), or control (n = 4). (**k**) Effect of morphine (escalating doses from 10 to 40 mg per kg intraperitoneally twice a day for 7 d) on mechanical sensitivity of TLR4-deficient C3H/HeJ mice (n = 11) and wild-type C3H/HeOuJ mice (n = 8). Mechanical sensitivity index was calculated as (10 − PW)/PW (10 = stimulations with 3.41 g–calibrated filament; PW = number of paw withdrawals). No differences were observed in the development of mechanical allodynia between mice groups (U = 30, P > 05). All threshold values were normalized to the baseline. Error bars in all panels represent s.e.m. n.s., not significant (P > 0.05; *P < 0.05; ***P < 0.001).

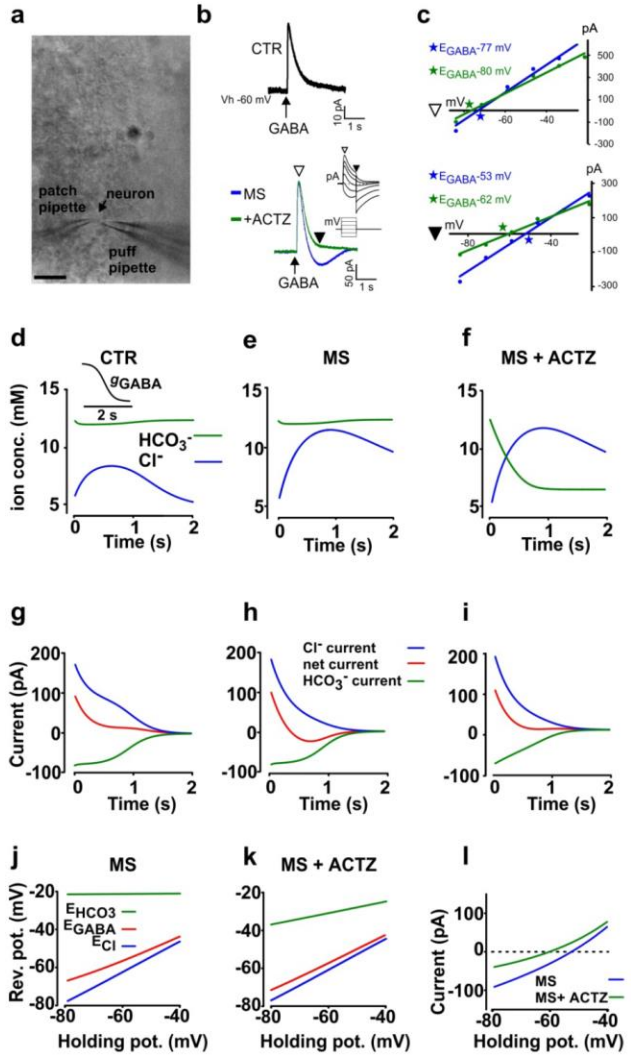

Supplementary Figure 1

Effects of the carbonic anhydrase (CA) inhibitor acetazolamide (ACTZ) on responses to prolonged activation of $GABA_A$ receptors analysed both experimentally and by computer simulations.

(**a-c**) ***Experimental data***: (**a**) Representative picture of a lamina I neuron showing the position of the recording and the puff pipettes (scale bar 15 µm). (**b**) Gramicidin-perforated patch clamp recording of GABA puff (arrow) responses obtained at -60 mV in control -*upper panel*- and from a morphine-treated lamina I neurons -*lower panel*- before (*in blue*) and after ACTZ (50 µM; *in green*; traces are scaled to the peak amplitude), as also shown in Figure 2h. Note the biphasic response in the morphine treated neurons *vs.* the monophasic response in ACTZ. This indicates a collapse in Cl current in response to GABA which unmasks a depolarizing $HCO3^-$ efflux. In the inset, a representative series of GABA responses superimposed on different steps in membrane potentials. (**c**) I-V curves measured at the peak of the response (*white arrowhead, top*) or 1 s after the GABA puff (*black arrowhead, bottom*) in the morphine-treated neuron before (*blue*) and after (*green*) ACTZ. Note the negligible shift in E_{GABA} induced by ACTZ when measured at the peak *vs.* the larger shift in E_{GABA} when measured 1 s after the GABA puff, indicating that the effect of ACTZ on anion homeostasis is activity-dependent. (**d-l**) ***Computer simulations***: (**d-f**) Time course of ion concentrations of Cl^- and $HCO3^-$ during a response to a puff of GABA in a model neuron in control condition (**d**), after morphine (**e**) and after morphine in the presence of ACTZ (**f**) at a holding potential of -60 mV. Ion concentrations were calculated by:

$$\frac{d[Cl^-]_i}{dt} = \frac{I_{Cl} + g_{KCC2}(E_K - E_{Cl})}{F \cdot Vol}$$

and $\frac{d[HCO_3^-]_i}{dt} = \frac{I_{HCO_3}}{F \cdot Vol} + ca([HCO_3^-]_i - [HCO_3^-]_{i,eq})$

where g_{KCC2} (0-5 nS) is the level of KCC2 activity, E_k (-90 mV) is the potassium reversal potential, *Vol* (1 X 10^{-10} cm^3) is the equivalent intracellular volume, *ca* (0-1X $10^6 s^{-1}$) is an index of CA activity and $[HCO3]_{i,eq}$ (12 mM) is the equilibrium intracellular $HCO3^-$ concentration. Inset in (**d**) shows the time course of the GABA conductance taking into account the following permeabilities:

$$P_{Cl} = P_{Cl,max}\left(1 + 0.1e^{\left(\frac{t-0.5}{0.2}\right)}\right)^{-1} \text{ and } P_{HCO3} = 0.25P_{Cl}.$$

ACTZ had a limited impact on the baseline value of $[HCO_3^-]_i$ (*e.g.*, at the onset of $GABA_A$ response). Yet, by blocking CA activity, ACTZ compromised the stability of $[HCO_3^-]_i$ during the response to GABA, allowing activity-dependent HCO3 - depletion (as seen after 1 s of $GABA_A$ activity). (**g-i**) Ionic currents carried by Cl- and HCO_3^- during a response to a puff of GABA in the model neuron in the same conditions as in (**d-f**). Ionic currents were computed with the Goldman- Hodgkin-Katz (GHK) flux equation at 293 K given a maximal permeability to Cl- ions $P_{Cl,max}$ = 1 X 10^{-15} m^3/s. (**h**) In conditions of impaired Clextrusion, the maintenance of $[HCO_3^-]_i$ allows the HCO_3^- current to parallel the $GABA_A$ conductance while the Cl- current collapses faster, yielding an inversion of the resulting $GABA_A$ current. (**i**) In the presence of ACTZ, the HCO_3^- current collapses faster than the $GABA_A$ conductance. The parallel collapse in Cl- and HCO_3^- currents prevents the development of the rebound inward $GABA_A$ current, restoring the ability of cells to maintain inhibition under sustained input. (**j-l**) The above simulations with different steps in membrane potentials as in (**a**); measurements were made at 1 s after the onset of the GABA puff. Values of E_{Cl}, E_{HCO3} and E_{GABA} were calculated from the Nernst and Goldman-Hodgkin-Katz equations for each membrane potential step in conditions of morphine (**j**) and morphine + ACTZ (**k**). (**j**) The timedependent collapse in $[HCO_3^-]_i$ varies as a function of the holding potential. (**k**) This dependency is stronger under ACTZ application. (**l**) A side effect of the change in E_{HCO3} (and hence E_{GABA}) as a function of time and holding potential (*Vh*) is an apparent change in $GABA_A$ conductance consistent with experimental observations in (**b-c**). Indeed, the slope conductance is given by by $g_{slope} = \Delta I / \Delta Vh$. Given that $I = g_{true}(Vh - E_{ion})$ and that E_{ion} is independent of *Vh*, we have $g_{slope} = g_{true}$. However, when E_{ion} depends on *Vh* (as in the present case), the conductance estimated from the slope between two holding potentials *V*1 and *V*2 is given by $g_{slope} - g_{true}(E_{ion}(V2) - E_{ion}(V1))(V2 - V1)^{-1}$, underestimating the true conductance.

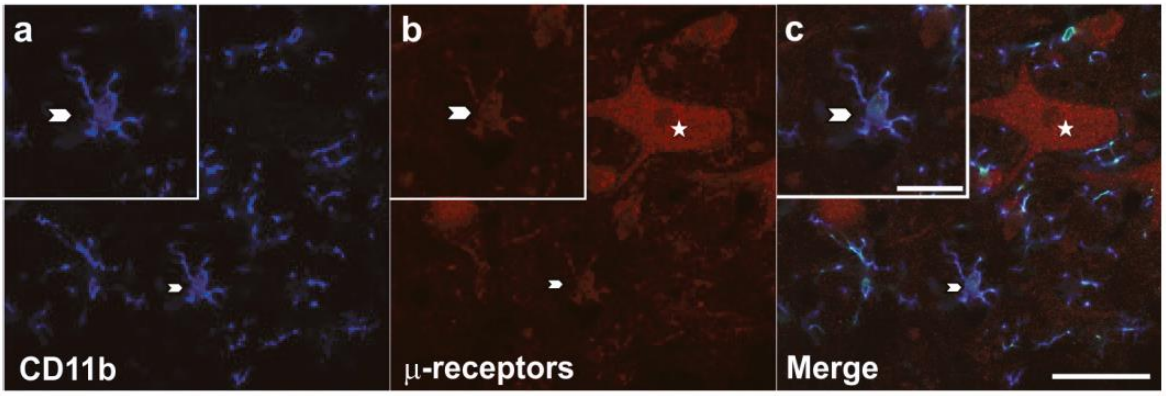

Supplementary Figure 2.
Expression of μ opioid receptor in spinal microglia. (**a**). Spinal microglia are double immunolabelled for the microglial marker CD11b (in *blue*). (**b**). Spinal μ-receptors are expressed in spinal neurons (*e.g.*, *star*) as well as in identified microglial cells (*e.g.*, *arrows*). (**c**) Merged fluorescent image. The insets show an enlargement of one of the doubled labeled microglial cells (arrows). Scale bar: 50 μm in the picture and 25 μm in the inset.

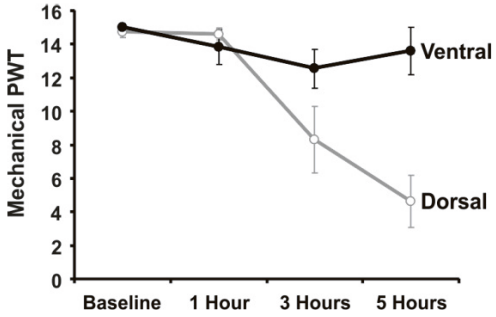

Supplementary Figure 3.
Activated microglia has a differential effect when injected dorsally or ventrally to the spinal cord**.** Paw withdrawal threshold (PWT, g) to mechanical stimuli before and after injection of activated microglia via intrathecal catheter. Data were separated based on whether the intrathecal catheter was found dorsal (n = 6) or ventral (n = 6) to the spinal cord after post-mortem examination.

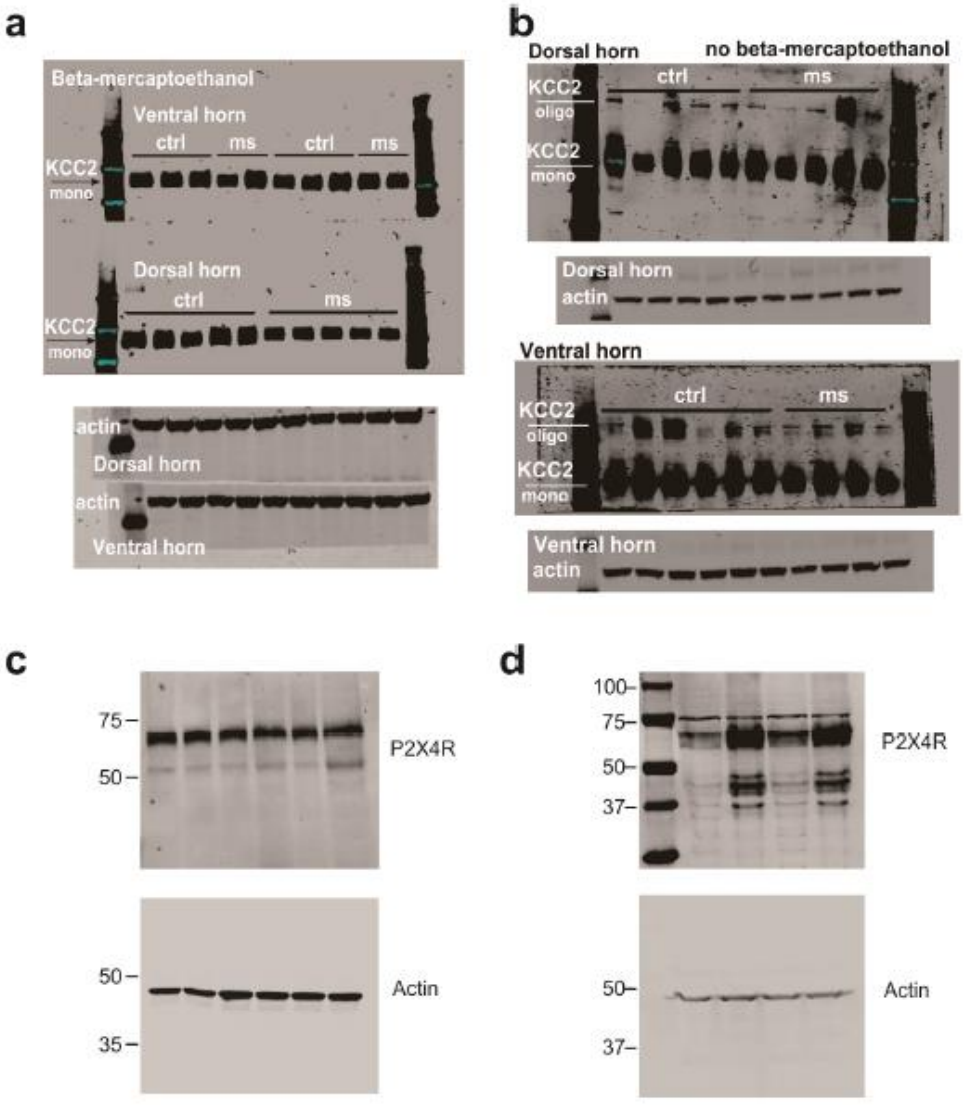

Supplementary Figure 4.
Full length western blots. **a-b.** Expression of KCC2 in the dorsal and ventral horn with and without betamercaptoethanol shown in Figure 3b,c. **c.** Expression of P2X4R in microglia cultures after morphine treatment shown in Figure 5i. **d.** Expression of P2X4R from spinal cords isolated from rats treated for 5 days with intrathecal saline, morphine, morphine+(-)NL, morphine+(+)NL shown in Figure 8h.